Title

author
certified by
accepted by
BIG BLANK PAGE
Title
by Matthew Greene
author in
submitted to BCS blah

abstract   1-pages of text

Acknowledgements

acknowledge 3 pages or so
BIG BLANK PAGE

Contents

Contents

List of Figures

Introduction

0.1 Retinal bipolar cells

Bipolar cells (BCs) provide the sole pathway from the photoreceptors of the retina to the amacrine and ganglion cells of the IPL. Since most amacrine cells (ACs) are inhibitory, and ganglion cells (GCs) do not synapse presynaptically within the IPL, BCs can be considered the primary source of excitatory input to the IPL.

Retinal bipolar cells were first subdivided into classes by the polarity of their central receptive field response (OFF or ON) [Werblin and Dowling(1969), Kaneko(1970)] or by whether their synapses with photoreceptors were "flat" or "invaginating" [Missotten(1965), Dowling and Boycott(1966)]. These classifications were initially thought to be related through observations in the cyprinid fish [Famiglietti et al.(1977)Famiglietti, Kaneko, and Tachibana], but it was soon discovered in amphibians that the relationship was not universal [Lasansky 1978]. Rodent work in the grey squirrel further cast doubt on the validity of the synaptic classification, as a class of BC in the squirrel retina was found to have both flat and invaginating synapses with cone photoreceptors [West(1978)].

Research in the late 1970s began to focus on classification using the depth of the stratification of the axonal arbor in the IPL [Famiglietti and Kolb(1976b)]. It was found that BCs with OFF centers stratify in the outer (proximal to the epithelium) region of the IPL, while BCs with ON centers stratify in the inner region. These outer and inner regions began to be referred to as subliminae a and b, respectively [Nelson et al.(1978)Nelson, Famiglietti, and Kolb]. The subdivision of BCs into more refined "types" demonstrates significant species difference. In the rabbit, it was observed through the reconstruction of individual neurons in electron micrograph images and through golgi staining that there existed at least nine distinct BC morphologies within the subliminae [Famiglietti(1981), Mills and Massey(1992)]. [Ghosh et al.(2004)Ghosh, Bujan, Haverkamp, Feig Extended this work to the mouse retina, wherein they identified nine cone BC types in addition to the rod BC using light microscopy with immunostaining to help distinguish cells with different receptor types. This classification was further refined by [Wässle et al.(2009)Wässle, Puller, Müller, and Haverkamp] using additional immunocytochemical markers, revealing that Type 3 (BC3) as defined by [Ghosh et al.(2004)Ghosh, Bujan, Haverkamp consisted of two separate types, BC3a and BC3b. They also hypothesized that BC5 was in fact two cell types, which was later confirmed by [Helmstaedter et al.(2013)Helmstaedter, Briggman, Turaga, through the dense reconstruction of electron micrograph images. [Helmstaedter et al.(2013)Helmstaedter, Br also identified a BC type that co-stratifies with the other BC5s, but has a wider lateral span and stratifies more narrowly in IPL depth, and they further speculated that there may exist a third BC5 type.

A BC type has several characteristics beyond mere anatomy, however, related to their

functional properties.

0.2 Early work on direction selectivity in retinal ganglion cells

Among the earliest work in the study of the behavior of cells in the vertibrate retina was that of Hartline in his 1938 account. Here it was discovered that there exists at least three types of retinal ganglion cells (GCs) that respond to different stimulus features. He identified ON cells that would respond to the onset of a light stimulus, OFF cells that would respond to the termination of light stimulation, and ON-OFF cells that respond to both the onset and termination of light. These observations were followed in the 1950s and early 1960s by several researchers, who demonstrated that there were units responding to more complicated features, such as convexity, dimming, and color specificity [Lettvin et al.(1959)Lettvin, Maturana, McCulloch, and Pitts, Wiesel(1960), Wolbarsht et al.(1961)Wolbarsht, Wagner, and MacNichol Jr]

[Barlow et al.(1964)Barlow, Hill, and Levick] were the first to discover directionally selective (DS) GCs. They observed a class of GC that responds to both ON and OFF stimuli that moves in a specific direction. They believed that DS arose in these cells through lateral inhibition displaced toward the preferred direction. If inhibition passes through a temporal delay line, or the inhibitory signal is sustained for a longer duration than the excitatory signal, this displacement could yield DS responses. [Wyatt and Daw(1975)] further investigated this theory and identified a cardioid-shaped inhibitory receptive field around each point of excitation on the DSGC, biased in the preferred direction.

Another model exists that has appeared in models of biological motion detection since the 1950s, but has not previously been ascribed to a specific neural circuit in the mammalian visual system. Motion can be detected by correlating excitatory input signals from two locations, if one signal passes through a temporal delay line. Stimulation of the delayed input followed by the nondelayed input causes signals to arrive synchronously at the output element, and to activate it. Stimulation in the opposite order gives rise to asynchronous signals at the output element, and no activation. In honor of the pioneering researcher Werner Reichardt, we will refer to the computational motif of Figure 1a as a "Reichardt detector," although it is actually a subunit of his model [Reichardt(1961)].

0.3 The starburst amacrine cells

In the 1980s, the starburst amacrine cell (SAC), a neuronal cell type in the mammalian retina, was discovered and characterized [Famiglietti(1983)]. SAC dendrites receive excitatory input synapses from bipolar cells (BCs), which in turn receive input from photoreceptors. SAC dendrites also make synapses onto ganglion cells [Famiglietti(1991)], which send signals from the retina to the brain through the optic nerve. Like most other amacrine cells, SACs lack an axon; their output synapses are found in the distal zones of their dendrites (Figure 1b).

There are two subtypes of SACs, one stratifying in the OFF sublayer of the IPL and one in the ON sublayer. The latter are sometimes called "displaced" SACs due to their somata appearing in the ganglion cell layer rather than the inner nuclear layer. The two types are morphologically very similar, although OFF SACs tend to be about 15% larger than their ON counterparts.

[Borg-Graham and Grzywacz(1992)] observed that SAC dendrites could function as temporal delay lines, as time is required for current from input synapses to propagate to output synapses (Figure 1c). They modeled SAC dendrites as passive electrical cables, and showed that temporal delays could lead to direction selectivity, as had been observed more generally by [Rall(1964)]. Their passive cable model can be approximated by a Reichardt detector, if BC input synapses onto an SAC dendrite are lumped into two groups: (1) proximal synapses near the soma, and (2) distal synapses near the dendritic tips and the output synapses (Figure 1c). Since proximal synapses are the delayed input and distal synapses the nondelayed input, [Borg-Graham and Grzywacz(1992)] predicted that outward motion should activate SAC dendrites more than inward motion.

Remarkably, their prediction of SAC direction selectivity was confirmed ten years later [Euler et al.(2002)Euler, Detwiler, and Denk], as well as their prediction of an outward "preferred direction" (PD). More recently, it was shown that BC inputs do not exhibit direction selectivity [Yonehara et al.(2013)Yonehara, Farrow, Ghanem, Hillier, Balint, Teixeira, Jüttner, Noda confirming their assumption that motion detection occurs somewhere between BCs and SACs.

However, an inconsistency with empirical data also emerged. According to the model, the soma should depolarize more for inward motion than for outward motion, i.e., have a PD opposite that of the distal dendrites. In fact, the PDs of the soma and distal zone turn out to be the same [Euler et al.(2002)Euler, Detwiler, and Denk]. To resolve this inconsistency, [Hausselt et al.(2007)Hausselt, Euler, Detwiler, and Denk] argued that active conductances must be added to the passive cable model of the SAC dendrite.

The passive cable model of SAC direction selectivity is based on the assumption that the temporal delay in the Reichardt detector is due to propagation of signals within the SAC dendrites. This paper explores another possibility: perhaps temporal delay could arise from mechanisms *presynaptic* to SAC dendrites (Figure 1d). Mouse BCs have been classified into multiple types [Wässle et al.(2009)Wässle, Puller, Müller, and Haverkamp], which are known to have distinct temporal behaviors [Baden et al.(2013)Baden, Berens, Bethge, and Euler, Borghuis et al.(2013)Borghuis, Marvin, Looger, and Demb]. If the connectivity of BC types with SACs varied with distance from the SAC soma, the BC-SAC circuit could end up resembling Figure 1d. We tested this hypothesis by reconstructing BC-SAC circuitry using e2198, a dataset of mouse retinal images from serial block-face scanning electron microscopy (SBEM) [Briggman et al.(2011)Briggman, Helmstaedter, and Denk].

Inhibitory connections between SACs are also known to exist [Lee and Zhou(2006)], and can contribute to SAC direction selectivity [Zhou and Lee(2008)]. However, SAC-SAC inhibition does not appear necessary for direction selectivity, which persists even during pharmacological blockade of inhibitory synaptic transmission [Hausselt et al.(2007)Hausselt, Euler, D Therefore the present work focuses on BC-SAC circuitry.

8

0.4 From onsac intro

The starburst amacrine cell (SAC) is a key player in retinal computation of the direction of a moving stimulus. Ablation of SACs impairs the optokinetic reflex, a behavior that depends on computation of visual motion [Yoshida et al.(2001)Yoshida, Watanabe, Ishikane, Tachibana, Pasta Amthor et al.(2002)Amthor, T, and Dmitrieva]. Both ablation [Yoshida et al.(2001)Yoshida, Watanabe, Ish Amthor et al.(2002)Amthor, T, and Dmitrieva] and reversible inactivation [Vlasits et al.(2014)Vlasits, Bos, of SACs reduce direction selective (DS) responses in ganglion cells, which receive synaptic input from SACs. SAC dendrites are preferentially activated by visual stimuli that move outward from the soma to the dendritic tips [Euler et al.(2002)Euler, Detwiler, and Denk, Lee and Zhou(2006), Hausselt et al.(2007)Hausselt, Euler, Detwiler, and Denk].

The proposed mechanisms for DS of SAC dendrites fall into several categories. According to inhibitory cellular hypotheses, dendritic biophysics causes inhibitory input to SACs to have effects that depend on dendritic location [Borg-Graham and Grzywacz(1992), Gavrikov et al.(2003)Gavrikov, Dmitriev, Keyser, and Mangel]. In inhibitory circuit hypotheses, GABAergic synaptic connectivity between SAC dendrites depends on the difference between their preferred directions [Lee and Zhou(2006), Münch and Werblin(2006)]. In excitatory cellular hypotheses, SAC biophysics causes excitatory input to SACs to have effects that depend on dendritic location [Tukker et al.(2004)Tukker, Taylor, and Smith, Hausselt et al.(2007)Hausselt, Euler, Detwiler, and Denk, Oesch and Taylor(2010)].

Recently we proposed a novel excitatory circuit hypothesis based on specificity of wiring between bipolar cells (BCs) and SACs. The proposal was based on anatomical evidence that sustained and transient BC types are connected to SACs at locations that are near and far from the SAC soma, respectively [Kim et al.(2014)Kim, Greene, Zlateski, Lee, Richardson, Turaga, I Such "space-time wiring specificity" could make the BC-SAC circuit function as a correlation-type motion detector [Borst and Euler(2011)], and is consistent with the observed outward preferred direction of SAC dendrites.

Like many other retinal neurons, the SAC comes in both On and Off types. The On SAC resembles a reflection of the Off SAC across a plane through the middle of the inner plexiform layer (IPL) (Fig. 1B, D). Probably due to this striking symmetry, DS and its mechanisms are often assumed to be similar between On and Off SACs. This remains merely an assumption as published studies of SACs were typically restricted to a single type. Physiological studies of DS were carried out for On SACs [Euler et al.(2002)Euler, Detwiler, and Denk, Lee and Zhou(2006), Hausselt et al.(2007)Hausselt, Euler, De while our anatomical study of BC-SAC wiring specificity was carried out for Off SACs [Kim et al.(2014)Kim, Greene, Zlateski, Lee, Richardson, Turaga, Purcaro, Balkam, Robinson, Behabadi, G

Here we find evidence that the On BC-SAC circuit possesses a space-time wiring specificity analogous to that shown previously for the Off BC-SAC circuit. We reconstructed a large set of On BCs and On SACs from e2198, a dataset of mouse retinal images from serial block-face scanning electron microscopy [Briggman et al.(2011)Briggman, Helmstaedter, and Denk]. Based on the resulting high-resolution information about the anatomy of single cells, we have succeeded in subdividing BC5 into three types that we call BC5t, BC5i, and BC5o. This finding confirms a speculation of [Helmstaedter et al.(2013)Helmstaedter, Briggman, Turaga, Jain, Seu who were previously able to distinguish just two BC5 types, but predicted the existence

of more. Our definition of a third BC5 type increases the total count of cone BC types to 13.

Contact analysis is consistent with a wiring diagram in which BC7 prefers to synapse closer to the On SAC soma, and BC5 prefers to synapse farther from the soma (Fig. 1C). Among the BC5 types, synaptic input from BC5o is likely to be less than from BC5t and BC5i.

Most of the available evidence suggests that transient BC types generally arborize near the IPL center, and sustained BC types near the IPL edges [Baden et al.(2013)Baden, Berens, Bethge, and E Borghuis et al.(2013)Borghuis, Marvin, Looger, and Demb]. (But see [Ichinose et al.(2014)Ichinose, Fyk-Ko for a divergent view.) Combined with the standard division of the IPL into On and Off sublamina, this yields four sublayers: On-sustained, On-transient, Off-transient, and Off-sustained (Fig. 1B). Based on this IPL organization, it is likely that BC7 is sustained and BC5 is transient. If this is the case, then On BC-SAC wiring is analogous to Off BC-SAC wiring.

0.5 from offsac intro

Compared to cognitive functions such as language, the visual detection of motion may seem trivial, yet the underlying neural mechanisms have remained elusive for half a century [Borst and Euler(2011), Vaney et al.(2012)Vaney, Sivyer, and Taylor]. Some retinal outputs (ganglion cells) respond selectively to visual stimuli moving in particular directions, while retinal inputs (photoreceptors) lack direction selectivity (DS). How does DS emerge from the microcircuitry connecting inputs to outputs?

Research on this question has converged upon the starburst amacrine cell (SAC, Figs. 1a, b). A SAC dendrite is more activated by motion outward from the cell body to the tip of the dendrite, than by motion in the opposite direction [Euler et al.(2002)Euler, Detwiler, and Denk]. Therefore a SAC dendrite exhibits DS, and outward motion is said to be its "preferred direction." Note that it is incorrect to assign a single such direction to a SAC, because each of the cell's dendrites has its own preferred direction (Fig. 1a). DS persists after blocking inhibitory synaptic transmission [Hausselt et al.(2007)Hausselt, Euler, Detwiler, and Denk], when the only remaining inputs to SACs are bipolar cells (BCs), which are excitatory. Since the SAC exhibits DS, while its BC inputs do not [Yonehara et al.(2013)Yonehara, Farrow, Ghanem, Hi we say that DS *emerges* from the BC-SAC circuit.

Mouse BCs have been classified into multiple types [Wässle et al.(2009)Wässle, Puller, Müller, and Haverk with different time lags in visual response [Baden et al.(2013)Baden, Berens, Bethge, and Euler, Borghuis et al.(2013)Borghuis, Marvin, Looger, and Demb]. Motion is a spatiotemporal phenomenon: an object at one location appears somewhere else after a time delay. Therefore we wondered whether DS might arise because different locations on the SAC dendrite are wired to BC types with different time lags. More specifically, we hypothesized that the proximal BCs (wired near the SAC soma) lag the distal BCs (wired far from the soma).

Such "space-time wiring specificity" could lead to DS as follows (Fig. 1c). Motion outward from the soma will activate the proximal BCs followed by the distal BCs. If

the stimulus speed is appropriate for the time lag, signals from both BC groups will reach the SAC dendrite simultaneously, summing to produce a large depolarization. For motion inward towards the soma, BC signals will reach the SAC dendrite asynchronously, causing only small depolarizations. Therefore the dendrite will "prefer" outward motion, as observed experimentally [Euler et al.(2002)Euler, Detwiler, and Denk].

1 Reconstruction of the Retina by Man and Machine

30 years ago, John Graham White, under the supervision of Sydney Brenner, undertook the heroic task of reconstructing the connectome of a tiny worm known as caenorhabditis elegans[White et al.(1986)White, Southgate, Thomson, and Brenner]. After a decade of labor, White produced the first connectome through almost entirely manual reconstruction. In some case, neural processes were even printed, and physical reconstructions were created as a means of visualization.

Happily, the development of modern computers allows us to substantially improve upon the reconstruction rate of White et al. We reconstructed e2198, an existing dataset of mouse retinal images from serial block-face scanning electron microscopy (SBEM) [Briggman et al.(2011)Briggman, Helmstaedter, and Denk]. The size of the data is approximately 350 μm x 350 μm x 50 μm, with the final dimension being parallel to the light axis. e2198 is located in the ventral portion of the retinal at a depth such that it spans the IPL and includes a portion of the INL and GCL.

1.1 Machine learning

The boundaries between neurons in subvolumes of the e2198 and e2006 datasets were manually traced. Using this as ground truth, a convolutional network (CN) was trained to detect boundaries between neurons using the MALIS method [Turaga et al.(2009)Turaga, Briggman, Helmst The CN had the same architecture as one used previously [Helmstaedter et al.(2013)Helmstaedter, Briggman and produced as output an affinity graph connecting nearest neighbor voxels [Turaga et al.(2010)Turaga, Mu Any subvolume of e2198 could be oversegmented by applying a modified watershed algorithm to the appropriate subgraph. The regions of the oversegmentation will be called supervoxels.

The e2198 dataset was oversegmented by an artificial intelligence (AI) into groups of neighboring voxels that were subsets of individual neurons. These "supervoxels" were assembled by humans into accurate 3D reconstructions of neurons. For this activity, we hired and trained a small number of workers in the lab, and also transformed work into play by mobilizing volunteers through EyeWire, a web site that turns 3D reconstruction of neurons into a game of coloring serial EM images.

1.2 Reconstruction by EyeWirers

Even before the learning in normal gameplay illustrated by Figure 2d, all EyeWirers are required to go through a training session immediately after registering for the site. This consists of a sequence of tutorial cubes, each of which was previously colored by an expert (Supplementary Figure 6). Each cube teaches through instructions and per-click feedback about accuracy based on comparing the EyeWirer's selections with those of the expert. After submitting a tutorial cube, the EyeWirer is given a chance to view mistakes.

Accuracy is monitored on a weekly basis by computing the precision and recall of each EyeWirer with respect to the truth, defined as neuron reconstructions based on EyeWire consensus followed by GrimReaper corrections. Less accurate EyeWirers are given less weight in the vote, which appears to improve the overall accuracy of the system.

Players' daily, weekly, and monthly scores are publicly displayed on a leaderboard (Supplementary Figure 7, right), motivating players to excel through competition. Players communicate with each other through online "chat" (Supplementary Figure 7, left) and discussion forums.

A "beta test" version of EyeWire was deployed in February 2012, and attracted a small group of users, who helped guide software development. After the official launch in December 2012, EyeWire was successful at reconstructing ganglion cells, but did not work well for reconstructing the more difficult SACs. In March 2013, EyeWirers were invited to the "Starburst Challenge," a sequence of tutorial cubes drawn from SACs. Those who passed with sufficient accuracy were an elite group allowed to reconstruct SACs (Supplementary Information).

Some SACs were reconstructed twice, once by workers and once by EyeWire.

1.3 Reconstruction by workers

A team of part-time workers, numbering about half a dozen at any given time, also reconstructed neurons using a more sophisticated version of the EyeWire interface. Workers were hired based on an interview and a short test of software use passed by 3/4 of the applicants. They were trained for 40 to 50 hours before generating reconstructions used for research. Their skills typically improved for months or even years after the initial training period, and were superior to those of professional neuroscientists without reconstruction experience.

As with EyeWire, the task of reconstructing an entire neuron was divided into subtasks, each of which involved reconstructing the neuron within a subvolume starting from a supervoxel "seed." However, the subvolumes were roughly 100 times larger than EyeWire cubes, and only two workers were assigned to each subvolume. In the first stage of error correction, disagreements were detected by computer, and resolved by one of the two workers, or a third worker. The third occasionally detected and corrected errors that were not disagreements between the first two. Most disagreements were the result of careless errors, and were easily resolved. More rarely, there were disagreements caused by

fundamental ambiguities in the image. These locations were noted for later examination with more contextual information, as described below.

In the second stage of error correction, 3D reconstructions of entire neurons were assembled from multiple subvolumes and inspected by one of the authors (J.S.K.). Suspicious branches or terminations, as well as overlaps between reconstructions of different neurons were detected. The original image was reexamined at these locations to check for errors. The process was repeated until no further errors could be detected. The F-score (Figure 2b) between the reconstructions before and after the second stage was 0.99 for SACs and 0.98 for BCs. Some errors may still remain, but it is likely that correcting them would have similarly little effect.

Through EyeWire, we wanted to enable anyone, anywhere, to participate in our research. The approach is potentially scalable to extremely large numbers of "citizen scientists" [Lintott et al.(2008)Lintott, Schawinski, Slosar, Land, Bamford, Thomas, Raddick, Nichol, Szalay, A More importantly, the 3D reconstruction of neurons requires highly developed visuospatial abilities, and we wondered whether a game could be more effective [Cooper et al.(2010)Cooper, Khatib, T than traditional methods of recruiting and creating experts.

In gameplay mode, EyeWire shows a 2D slice through a "cube," an e2198 subvolume of 256^3 grayscale voxels (Fig. 2a). Gameplay consists of two activities: coloring the image near some location, or searching for a new location to color. Coloring is done by clicking at any location in the 2D slice, which causes the supervoxel containing that location to turn blue. Searching is done by translating and orienting the slice within the cube, and interacting with a 3D rendering of the colored supervoxels.

When the player first receives a cube, it already comes with a "seed," a contiguous set of colored supervoxels. The challenge is to color all the rest of the supervoxels that belong to the same neuron, and avoid coloring other neurons. Gameplay for a cube terminates when the player clicks "Submit," receives a numerical score (Extended Data Fig. 1a), and proceeds to the next cube. Because our AI is sufficiently accurate, coloring supervoxels is faster than manually coloring voxels, an older approach to 3D reconstruction [Fiala(2005)].

The scoring system is designed to reward accurate coloring. This is nontrivial because EyeWire does not know the correct coloring. Each cube is assigned to multiple players (typically 5 to 10), and high scores are earned by players who color supervoxels that other players also color. In other words, the scoring system rewards agreement between players, which tends to be the same as rewarding accuracy.

Consensus is used not only to incentivize individual players, but also to enhance the accuracy of the entire system. Any player's coloring is equivalent to a set of supervoxels. Given the colorings of multiple players starting from the same seed in the same cube, a consensus can be computed by voting on each supervoxel. EyeWirer consensus was much more accurate than any individual EyeWirer (Fig. 2b,c).

Coloring a neuron is more challenging than it sounds. Images are corrupted by noise and other artifacts. Neurites take paths that are difficult to predict, and can branch without warning. Careless errors result from lapses in attention. Extensive practice is required to achieve accuracy. The most accurate EyeWirers (Fig. 2c, upper right corner) often had experience with thousands of cubes. Improvements in accuracy were

observed over the course of hundreds of cubes, corresponding to tens of hours of practice (Fig. 2d). According to subjective reports of EyeWirers, learning continues for much longer than that. In contrast, previous successes at "crowdsourcing" image analysis involved tasks that did not require such extensive training [Von Ahn and Dabbish(2004), Lintott et al.(2008)Lintott, Schawinski, Slosar, Land, Bamford, Thomas, Raddick, Nichol, Szalay, Andreesc

Reconstructing an entire neuron requires tracing its branches through thousands of cubes. This process is coordinated by an automatic spawner, which inspects each consensus cube for branches that exit the cube. Each exit generates a new cube and seed, which are added to a queue. EyeWirers are automatically assigned to cubes by an algorithm that attempts to balance the number of plays for each cube.

Over 100,000 registered EyeWirers have been recruited by news reports, social media, and the EyeWire blog. Players span a broad range of ages and educational levels, come from over 130 countries, and the great majority have no formal training in neuroscience (Extended Data Figs. 2 and 3; Supplementary Notes). These statistics show that Eye-Wire indeed widens participation in neuroscience research. At the same time, the most avid players constitute an elite group with disproportionate achievements. For example, the top 100 players have contributed about half of all cubes completed in EyeWire.

Lab workers also reconstructed neurons independently of EyeWire, with a more sophisticated version of the user interface (Methods). Their reconstructions were pooled with those of EyeWirers for the analyses reported below. Reconstruction error was quantified (Methods), and was treated like other kinds of experimental error when calculating confidence intervals from our data.

Reconstruction of Off SACs Off SACs were reconstructed by (1) forward tracing from the soma to dendritic tips and (2) backward tracing from varicosities on candidate SAC dendrites to the soma. In the forward method, a candidate SAC soma was identified as a supervoxel with a characteristic pattern of dendritic stubs bearing spiny protrusions. By the time reconstruction progressed to approximately half of the average SAC radius, an Off SAC could be conclusively recognized by its starburst shape and narrow stratification at the appropriate IPL depth. More than 90% of candidates turned out to be SACs.

In the backward method, we located a thin dendrite with varicosities at the appropriate IPL depth. This was reconstructed back to the soma, and then the rest of the dendrites were reconstructed from the soma to the tips. The cell could be discarded at any point during this process, if its dendrites escaped from the appropriate IPL depth or failed to exhibit the proper morphological characteristics. Less than 25% of initial candidates ended up confirmed as SACs.

In total, 79 Off SACs were reconstructed, 39 by forward tracing and 52 by backward tracing. After candidates were identified by one of the authors (J.S.K.), reconstructions were performed by lab workers (59 cells) or by EyeWirers (29 cells). Overlapping numbers (12 for forward/backward, 9 for workers/EyeWirers) mean the combination of the two.

Reconstruction of Off BCs Because only part of the inner nuclear layer (INL) was encompassed in e2198, the somata of Off bipolar cells (BCs) were generally outside the

dataset. Therefore we searched the INL for candidate BC axons traveling between the somata, and traced them into the INL. Those that arborized in the Off region of the INL were further reconstructed. Cells that violated known BC structures were identified as amacrine cells and discarded [Helmstaedter et al.(2013)Helmstaedter, Briggman, Turaga, Jain, Seung, and I

BC axons were difficult to reconstruct due to poor staining, and their highly irregular shapes. They could not be accurately reconstructed (either by online volunteers or lab experts) within the 256^3 cubes of EyeWire, which were too small to provide sufficient spatial context. Therefore BCs were reconstructed only by lab workers using the large subvolumes mentioned above.

SAC reconstruction

On SACs were reconstructed mostly during July 2013 to September 2014. EyeWirers who helped reconstruct On SACs are listed in the Supplemental Information.

Off SACs were previously reconstructed both by forward tracing from the candidate SAC soma to dendritic tips, and backward tracing from varicosities on candidate SAC dendrites to the soma [Kim et al.(2014)Kim, Greene, Zlateski, Lee, Richardson, Turaga, Purcaro, Balkam, I The forward method turned out to be less useful for On SACs because their dendrites can take rather circuitous paths before reaching their final IPL depth and making the distinctive starburst shape. Therefore it takes a great deal of reconstruction effort before a candidate cell can be accepted or rejected as a SAC. It saves human effort if this decision can be made earlier in the reconstruction process. Two On SACs were reconstructed by lab workers using the forward method. The remaining 75 were reconstructed by EyeWirers using the backward method.

In a parallel study to be reported elsewhere, we exhaustively reconstructed all neurons with somata in a $(200 \, \mu\text{m})^2$ GCL patch of e2198. This revealed 6 extra On SACs beyond the 35 in the patch that had already been reconstructed for the present study. In other words, the reconstructions of the present study had achieved 85% coverage of all On SACs in this $(200 \, \mu\text{m})^2$ patch. Assuming that the density of On SACs is the same for all of e2198 as it is in the $(200 \, \mu\text{m})^2$ patch, the estimated number of On SACs in e2198 is roughly 110, and our overall coverage is roughly 70%. Our estimated coverage of Off SACs is slightly lower, as the Off SAC density is known to be slightly (less than 10%) larger than the On SAC density [Jeon et al.(1998)Jeon, Strettoi, and Masland].

SAC properties

Length of SAC dendrites (Fig. 2E inset) was calculated as the mean distance from the soma on the xy plane of the eight most distant points that are not within $30 \, \mu\text{m}$ of each other. These parameters were chosen because the points generated appeared to give an accurate representation of the dendritic length, while avoiding inaccuracy that arises from outliers and from dendrites that extend beyond the bounds of the volume.

BC reconstruction

On BCs were reconstructed mostly during February to December 2014. Because e2198 extends only partially into the INL, it was not possible to identify BCs based on the existence of a dendritic arbor in the OPL. Instead, we identified BC axonal arbors by comparison with [Helmstaedter et al.(2013)Helmstaedter, Briggman, Turaga, Jain, Seung, and Denk], who reconstructed all BCs in a patch of retina that included both IPL and OPL. BC axon candidates were neurites that pass through the interstices of the INL and emerge in the IPL. Many candidates could be immediately rejected as amacrine or ganglion cells because their arbors were too large, or rejected as glial cells based on surface concavity and roughness. Little human effort was necessary for these cases, because large parts of these cells were automatically reconstructed. The remaining candidates were put into the reconstruction pipeline, and were rejected as narrow field amacrine cells if their stratification profiles deviated markedly from those previously reported by [Helmstaedter et al.(2013)Helmstaedter, Briggman, Turaga, Jain, Seung, and Denk] for BCs. Eight were rejected in the middle of reconstruction, and three were rejected after full reconstruction.
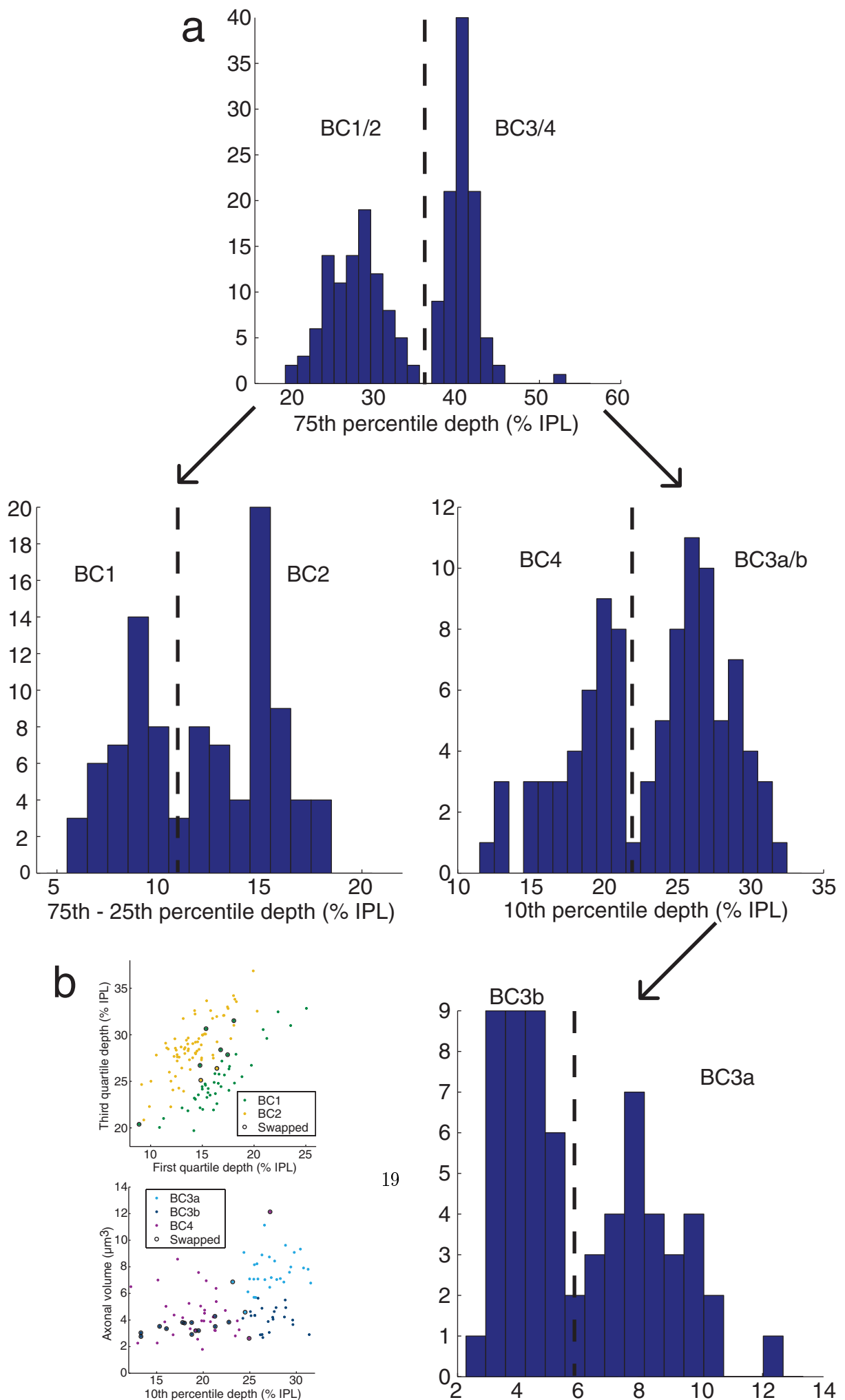
2 Classification of Bipolar Cells

asdasd

2.1 Classification of Off Bipolar by Morphology

BC stratification profiles were computed by dividing surface voxels into 100 bins spanning 0 to 100% IPL depth. Classification into cell types was done by using methods similar to those described previously [Helmstaedter et al.(2013)Helmstaedter, Briggman, Turaga, Jain, Seung, and De The BCs were split into shallow (BC1/2) and deep (BC1/2) clusters using the 75th percentile depth of the stratification profile. The BC1/2 cluster was further subdivided by stratification width, defined as the difference between 75th and 25th percentile depths. The wider cluster was identified as BC2 and the narrower cluster as BC1, based on a molecular classification showing that BC2 has more cells per square millimeter than BC1 [Wässle et al.(2009)Wässle, Puller, Müller, and Haverkamp]. This correspondence between structural and molecular classifications is the opposite of a previous report [Helmstaedter et al.(2013)Helmstaedter, Briggman, Turaga, Jain, Seung, and Denk]. The discrepancy may be due to methodological differences, such as computing stratification profiles based on surface voxels versus skeletons. The BC3/4 cluster was subdivided into BC4 and BC3 by the 10th percentile depth, because the molecularly defined BC4 stratifies closer to the INL [Wässle et al.(2009)Wässle, Puller, Müller, and Haverkamp]. Finally, BC3 was subdivided into BC3a and BC3b based on axonal arbor volume, with BC3a having the larger axonal volume. Supplementary Figure xxx shows that each of the above subdivision steps was based on a feature with a roughly bimodal histogram.

The result still contained a small number of classification errors, as adjacent BCs of the same type overlapped enough to violate the mosaic property. Corrections were made by an automatic algorithm that greedily swapped cells from one cluster to another such that the total overlap between convex hulls of cells of a given type was minimized. Two swaps were vetoed by an expert (J.S.K) on the basis of morphological features. In all, six cells were swapped within BC1/2 and 13 within BC3/4. In the final classification, 41, 56, 29, 35, and 34 BCs were identified as types 1, 2, 3a, 3b, and 4, respectively (Supplementary Figure 2a-e, Supplementary Table 1). A few cells that violated the mosaic of all types and had irregular stratification profiles were discarded as possible reconstruction errors or amacrine cells.

2.2 Classification of On Bipolar by Morphology

We define the stratification profile as the density of surface area versus depth in the IPL. For the purpose of BC classification, we restricted the domain of the stratification profile to the interval between IPL depth 0.4 and 1. The domain omitted depths between 0 and 0.4 to exclude the trunks of the axonal arbors, which increase variability of the stratification profiles. Each stratification profile is normalized like a probability density, so that profile area between IPL depths 0.4 and 1 integrates to unity. Since IPL depth is dimensionless, the stratification profile is also dimensionless. [Helmstaedter et al.(2013)Helmstaedter, Briggman, T defined stratification profile as the density of reconstructed skeleton. This definition is slightly different from ours, but yields similar results (data not shown). Percentiles are defined for a stratification profile, in the same way as for a probability density. Namely, the interval from the nth percentile depth to 0th percentile depth contains n percent of the area of the stratification profile. As mentioned earlier, 0th percentile depth is defined as IPL depth 0.4. The thickness of the stratification profile is defined as the difference between 85th and 25th percentile depths. [Helmstaedter et al.(2013)Helmstaedter, Briggman, Turaga, Jain, Se defined thickness as the difference between 75th and 25th percentile depths, which yields similar classifications. In addition to stratification, we characterized single cell anatomy by a further property, the area of the cell's projection onto the tangential (xy) plane.

We hierarchically clustered our On BCs as follows. The axonal arbors of BC5 and XBC lie between the Off and On SACs. Accordingly, a BC5/XBC cluster separates from other types based on 85th percentile depth (Figure S1A). This cluster in turn subdivides by 25th percentile depth into outer (closer to the INL) and inner (closer to the GCL) clusters (Figure S1B). The outer cluster can be divided into BC5t and BC5o; the former is more thickly stratified than the latter (Figure S1D). The inner cluster divides into XBC and BC5i based on projection area (Figure S1E).

Types outside the BC5/XBC cluster lie between the On SACs and GCL. BC7 separates from the others by 85th percentile depth (Figure S1A). Then BC6, BC8/9, and RBC separate from each other based on projection area (Figure S1C). We chose not to separate BC8 and BC9, as the reconstructed cells were too few to yield two complete tilings.

BC8, BC9, and RBC all appear underrepresented relative to [Helmstaedter et al.(2013)Helmstaedter, Brigg This discrepancy could be artifactual, caused by failures to identify the relatively thin axons of these three types in the interstices of the INL. Alternatively, these cell types might be truly underrepresented in our volume.

Histograms showing the various splits in the hierarchical clustering are shown in Figure S1. The splits are highly convincing near the top of the hierarchy, but less convincing near the bottom. Therefore we sought further validation from the principle that the arbors of a bipolar cell type should "tile" the retina with little overlap. If the hierarchical clustering yields cell types that tile the retina, that would be independent validation of the clustering, which relied only on anatomical properties of single cells. For all types, few violations of the tiling principle were observed (Figure 3E, F, G). There are some holes in the tilings, but they are likely the result of omissions in cell reconstruction rather than classification errors. Violations of tiling can be rectified by swapping cells between types, to yield the improved classifications given in Fig. S3. The fraction of swapped

cells is small (Table S1). Our final classification is exhibited in the "type gallery" of Fig. S3.
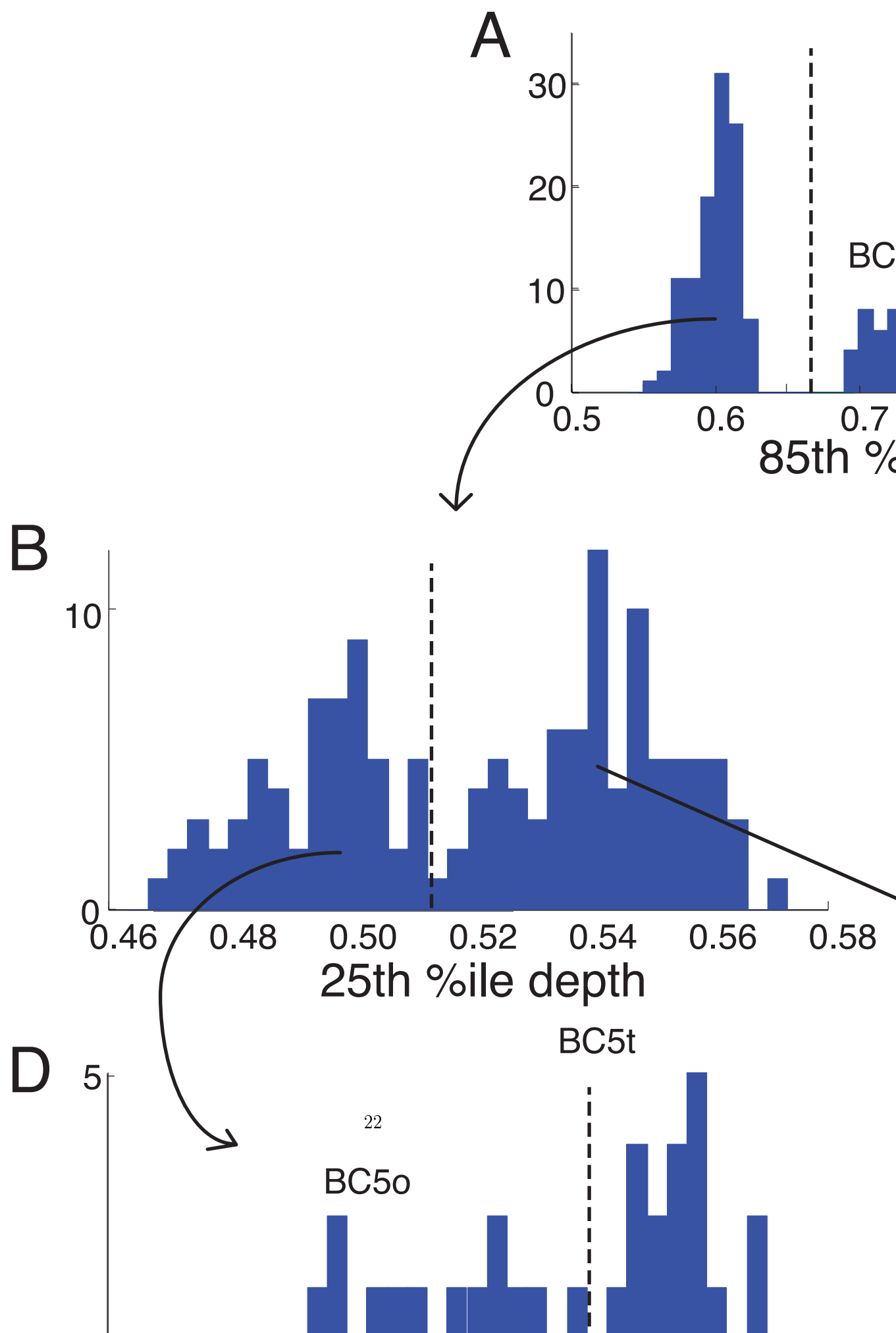
2.3 Connectivity-based Classification

Only if the stratification profiles of two cells overlap is there potential for contact between the cells, and hence potential for synaptic connections. In other words, stratification constrains retinal connectivity [Masland(2004)]. It follows that cell types defined using stratification are likely to end up having functional significance, assuming that the connectivity of a cell is closely related to its function [Seung and Sümbül(2014)].

It would be more direct to define a cell type as a set of cells with similar contact or connectivity patterns [Seung(2009), Seung(2012)], rather than use stratification as a proxy for these properties. For example, the 302 neurons of *C. elegans* were divided into 118 classes, each containing neurons with similar connectivity patterns [White et al.(1986)White, Southgate, Thomson, and Brenner]. Likewise [Helmstaedter et al.(2013)Helmsta divided BC5 into classes based on patterns of contact with two ganglion cell types named "gc31-56" and "gc36-51." We decided to replicate their analysis, mainly in order to determine the correspondence between contact-based and stratification-based classifications. A secondary motivation was to examine how contact-based classification depends on the completeness of reconstruction. [Helmstaedter et al.(2013)Helmstaedter, Briggman, Turaga, Jain, Seung, an reconstructed all neurons with cell bodies contained in a $(0.1 \text{ mm})^2$ patch. This method missed ganglion cells with arbors inside the patch but cell bodies outside the patch, which is why gaps in coverage are visible in the gallery of cell types provided in the Supplementary Data of [Helmstaedter et al.(2013)Helmstaedter, Briggman, Turaga, Jain, Seung, and Denk]. Contact with missing arbors obviously cannot be quantified, hampering contact-based classification.

We were able to replicate and improve the contact-based classification by making use of a large set of ganglion cells that were reconstructed from the e2198 dataset in a parallel study to be reported elsewhere. From this set of ganglion cells, we identified 16 examples of gc31-56 and 19 examples of gc36-51 based on their distinctive stratification profiles (Figs. 4A, B). The arbors of each ganglion cell type completely cover the central region of e2198 where the bipolar cells are located, because the reconstructed ganglion cells include those with cell bodies outside the central region (Fig. S3). For each BC5 cell, we quantified the fraction of its axonal surface area in contact with gc31-56 cells, and the fraction of its axonal area in contact with gc36-51 cells. Then BC5 indeed splits nicely into two clusters based on the two contact fractions (Fig. 4C). One cluster, named "BC5A" by [Helmstaedter et al.(2013)Helmstaedter, Briggman, Turaga, Jain, Seung, and Denk], has more contact with gc31-56. BC5A tiles with few violations (Fig. 4E) and therefore appears to be a pure cell type. BC5A corresponds almost exactly with BC5i (Fig. 4C).

The other cluster, named "BC5R" by [Helmstaedter et al.(2013)Helmstaedter, Briggman, Turaga, Jain, Se has more contact with gc36-51. Because BC5R contains many tiling violations (Fig. 4E), [Helmstaedter et al.(2013)Helmstaedter, Briggman, Turaga, Jain, Seung, and Denk] speculated that BC5R was a mixture of more than one type. Our stratification-based clas-

A

30

20

10

0

BC

0.5   0.6   0.7

85th %

B

10

0

0.46   0.48   0.50   0.52   0.54   0.56   0.58

25th %ile depth

BC5t

D   5

22

BC5o

sification confirms their speculation by effectively dividing BC5R into BC5o and BC5t, both of which tile the retina separately.

The cleanness of the division between BC5A and BC5R is evident in a histogram of the difference between the gc31-56 and gc36-51 contact fractions, in which two well-separated clusters are evident (Fig. 4D). Note that [Helmstaedter et al.(2013)Helmstaedter, Briggman, Turaga, Jain, S labeled some of their reconstructed cells as BC5X. This name was not intended to be a type but rather indicated cells that were unclassifiable because they lacked contact with gc31-56 and gc36-51. We do not have this problem because our coverage of the ganglion cell types is more complete.

3 Direction Selectivity in the Off SAC

Compared to cognitive functions such as language, the visual detection of motion may seem trivial, yet the underlying neural mechanisms have remained elusive for half a century [Borst and Euler(2011), Vaney et al.(2012)Vaney, Sivyer, and Taylor]. Some retinal outputs (ganglion cells) respond selectively to visual stimuli moving in particular directions, while retinal inputs (photoreceptors) lack direction selectivity (DS). How does DS emerge from the microcircuitry connecting inputs to outputs?

Research on this question has converged upon the starburst amacrine cell (SAC, Figs. 1a, b). A SAC dendrite is more activated by motion outward from the cell body to the tip of the dendrite, than by motion in the opposite direction [Euler et al.(2002)Euler, Detwiler, and Denk]. Therefore a SAC dendrite exhibits DS, and outward motion is said to be its "preferred direction." Note that it is incorrect to assign a single such direction to a SAC, because each of the cell's dendrites has its own preferred direction (Fig. 1a). DS persists after blocking inhibitory synaptic transmission [Hausselt et al.(2007)Hausselt, Euler, Detwiler, and Denk], when the only remaining inputs to SACs are bipolar cells (BCs), which are excitatory. Since the SAC exhibits DS, while its BC inputs do not [Yonehara et al.(2013)Yonehara, Farrow, Ghanem, Hi we say that DS *emerges* from the BC-SAC circuit.

Mouse BCs have been classified into multiple types [Wässle et al.(2009)Wässle, Puller, Müller, and Haverk with different time lags in visual response [Baden et al.(2013)Baden, Berens, Bethge, and Euler, Borghuis et al.(2013)Borghuis, Marvin, Looger, and Demb]. Motion is a spatiotemporal phenomenon: an object at one location appears somewhere else after a time delay. Therefore we wondered whether DS might arise because different locations on the SAC dendrite are wired to BC types with different time lags. More specifically, we hypothesized that the proximal BCs (wired near the SAC soma) lag the distal BCs (wired far from the soma).

Such "space-time wiring specificity" could lead to DS as follows (Fig. 1c). Motion outward from the soma will activate the proximal BCs followed by the distal BCs. If the stimulus speed is appropriate for the time lag, signals from both BC groups will reach the SAC dendrite simultaneously, summing to produce a large depolarization. For motion inward towards the soma, BC signals will reach the SAC dendrite asynchronously, causing only small depolarizations. Therefore the dendrite will "prefer" outward motion, as observed experimentally [Euler et al.(2002)Euler, Detwiler, and Denk].

3.1 3D reconstruction by crowd and machine

We tested our hypothesis by reconstructing Off BC-SAC circuitry using e2198, an existing dataset of mouse retinal images from serial block-face scanning electron microscopy (SBEM) [Briggman et al.(2011)Briggman, Helmstaedter, and Denk]. The e2198 dataset

was oversegmented by an artificial intelligence (AI) into groups of neighboring voxels that were subsets of individual neurons. These "supervoxels" were assembled by humans into accurate 3D reconstructions of neurons. For this activity, we hired and trained a small number of workers in the lab, and also transformed work into play by mobilizing volunteers through EyeWire, a web site that turns 3D reconstruction of neurons into a game of coloring serial EM images.

Through EyeWire, we wanted to enable anyone, anywhere, to participate in our research. The approach is potentially scalable to extremely large numbers of "citizen scientists" [Lintott et al.(2008)Lintott, Schawinski, Slosar, Land, Bamford, Thomas, Raddick, Nichol, Szalay, A More importantly, the 3D reconstruction of neurons requires highly developed visuospatial abilities, and we wondered whether a game could be more effective [Cooper et al.(2010)Cooper, Khatib, 7 than traditional methods of recruiting and creating experts.

In gameplay mode, EyeWire shows a 2D slice through a "cube," an e2198 subvolume of 256^3 grayscale voxels (Fig. 2a). Gameplay consists of two activities: coloring the image near some location, or searching for a new location to color. Coloring is done by clicking at any location in the 2D slice, which causes the supervoxel containing that location to turn blue. Searching is done by translating and orienting the slice within the cube, and interacting with a 3D rendering of the colored supervoxels.

When the player first receives a cube, it already comes with a "seed," a contiguous set of colored supervoxels. The challenge is to color all the rest of the supervoxels that belong to the same neuron, and avoid coloring other neurons. Gameplay for a cube terminates when the player clicks "Submit," receives a numerical score (Extended Data Fig. 1a), and proceeds to the next cube. Because our AI is sufficiently accurate, coloring supervoxels is faster than manually coloring voxels, an older approach to 3D reconstruction [Fiala(2005)].

The scoring system is designed to reward accurate coloring. This is nontrivial because EyeWire does not know the correct coloring. Each cube is assigned to multiple players (typically 5 to 10), and high scores are earned by players who color supervoxels that other players also color. In other words, the scoring system rewards agreement between players, which tends to be the same as rewarding accuracy.

Consensus is used not only to incentivize individual players, but also to enhance the accuracy of the entire system. Any player's coloring is equivalent to a set of supervoxels. Given the colorings of multiple players starting from the same seed in the same cube, a consensus can be computed by voting on each supervoxel. EyeWirer consensus was much more accurate than any individual EyeWirer (Fig. 2b,c).

Coloring a neuron is more challenging than it sounds. Images are corrupted by noise and other artifacts. Neurites take paths that are difficult to predict, and can branch without warning. Careless errors result from lapses in attention. Extensive practice is required to achieve accuracy. The most accurate EyeWirers (Fig. 2c, upper right corner) often had experience with thousands of cubes. Improvements in accuracy were observed over the course of hundreds of cubes, corresponding to tens of hours of practice (Fig. 2d). According to subjective reports of EyeWirers, learning continues for much longer than that. In contrast, previous successes at "crowdsourcing" image analysis involved tasks that did not require such extensive training [Von Ahn and Dabbish(2004),

Lintott et al.(2008)Lintott, Schawinski, Slosar, Land, Bamford, Thomas, Raddick, Nichol, Szalay, Andrees

Reconstructing an entire neuron requires tracing its branches through thousands of cubes. This process is coordinated by an automatic spawner, which inspects each consensus cube for branches that exit the cube. Each exit generates a new cube and seed, which are added to a queue. EyeWirers are automatically assigned to cubes by an algorithm that attempts to balance the number of plays for each cube.

Over 100,000 registered EyeWirers have been recruited by news reports, social media, and the EyeWire blog. Players span a broad range of ages and educational levels, come from over 130 countries, and the great majority have no formal training in neuroscience (Extended Data Figs. 2 and 3; Supplementary Notes). These statistics show that EyeWire indeed widens participation in neuroscience research. At the same time, the most avid players constitute an elite group with disproportionate achievements. For example, the top 100 players have contributed about half of all cubes completed in EyeWire.

Lab workers also reconstructed neurons independently of EyeWire, with a more sophisticated version of the user interface (Methods). Their reconstructions were pooled with those of EyeWirers for the analyses reported below. Reconstruction error was quantified (Methods), and was treated like other kinds of experimental error when calculating confidence intervals from our data.

3.2 Contact analysis

We reconstructed 195 Off BC axons and 79 Off SACs from e2198 (Fig. 3b, Extended Data Fig. 4). The e2198 retina was stained in an unconventional way that did not mark intracellular structures such as neurotransmitter vesicles [Briggman et al.(2011)Briggman, Helmstaedter, and Der and reliable morphological criteria for identification of BC presynaptic terminals are unknown. As an indirect measure of connectivity, contact areas were computed for all BC-SAC pairs. The resulting "contact matrix" was analyzed through two subsequent steps.

In the first step, Off BC axons were classified into five cell types, following structural criteria [Helmstaedter et al.(2013)Helmstaedter, Briggman, Turaga, Jain, Seung, and Denk] established to correspond with previous molecular definitions [Wässle et al.(2009)Wässle, Puller, Müller, and (Methods, Extended Data Fig. 5). BC types stratify at characteristic depths in the inner plexiform layer (IPL), and vary in size (Fig. 4a). The BCs of each type formed a "mosaic," meaning that cells were spaced roughly periodically (Extended Data Fig. 6a-e). This is generally accepted as an important defining property of a retinal cell type. Type densities (Extended Data Fig. 6f) were roughly consistent with previous reports [Wässle et al.(2009)Wässle, Puller, Müller, and Haverkamp]. When the columns of the contact matrix were sorted by BC type (Fig. 4b), it became evident that BC2 and BC3a contact SACs more than other BC types.

In the second step, we averaged contact area over BC-SAC pairs of the same BC type and similar distance between the BC axon and the SAC soma in the plane tangential to the retina (Fig. 4c). These absolute areas were normalized to convert them into the percentage of SAC surface area covered by BCs of a given type (Methods). The resulting

graphs show that BC2 prefers to contact SAC dendrites close to the SAC soma, whereas BC3a prefers to contact far from the soma (Fig. 4d, Extended Data Fig. 7c).

Imaging of intracellular calcium in BC axons [Baden et al.(2013)Baden, Berens, Bethge, and Euler] and extracellular glutamate around BC axons [Borghuis et al.(2013)Borghuis, Marvin, Looger, and Demb] indicate that BC2 lags BC3a in visual responses by 50 to 100 ms. Therefore BC-SAC wiring appears to possess the space-time specificity appropriate for an outward preferred direction, as we hypothesized (Fig. 1c).

3.3 Co-stratification analysis

Off SACs stratify at a particular depth in the IPL (Fig. 1b). Why this depth and not some other? From Fig. 4a, it is obvious that this depth is appropriate for wiring with BC2 and BC3a, as required by our model of DS emergence. Following this logic one step further, we wondered whether the observed dependence of contact on distance from the SAC soma might be reflected in fine aspects of SAC morphology. We hypothesized that SAC dendrites are "tilted," moving deeper into the IPL with distance from the SAC soma. Such a change in depth would be compatible with more overlap with BC2 near the soma, and more overlap with BC3a far from the soma, since BC3a is deeper in the IPL than BC2 (Fig. 4a and Supplementary Video).

The hypothesized tilt turns out to exist (Fig. 5a). Very close to the SAC soma, the dendrites dive sharply into the IPL from the INL. Surprisingly, IPL depth continues to increase as distance from the SAC soma in the tangential plane ranges from 20 to 80 μm. The slight increase is not evident in a single dendrite (Fig. 1b), but emerges from statistical averaging.

Could dendritic tilt be the cause of the observed variation in BC-SAC contact with distance (Fig. 4d)? We cannot address causality based on our data, but we can test how well the tilt predicts contact variation. We computed the stratification profiles of BC types (Fig. 5a), defined as the one-dimensional density of BC surface area along the depth of the IPL. We also computed the stratification profile of SAC dendrites at various distances from the SAC soma (quartiles, Fig. 5a). Assuming that BC and SAC arbors are statistically independent of each other, we estimated contact from "co-stratification," defined as the integral over IPL depth of the product of BC and SAC stratification profiles (Methods).

We found that actual BC2 contact depends more strongly on distance than predicted; the slight change in IPL depth after the initial plunge appears too small to account for the large change in actual BC2 contact. In other failures of contact prediction, BC3a, BC3b, and BC4 stratify at the same IPL depths (Fig. 5a), yet BC3a makes much more contact than BC3b or BC4. Also, actual BC3a contact plummets near the tips of SAC dendrites (Fig. 4d), while predicted contact does not change at all because the IPL depth of SAC dendrites is constant in this region (Fig. 5b). Overall, the total contact from all BC types seems low in this region (Extended Data Fig. 7d), suggesting that BCs avoid making synaptic inputs to the most distal SAC dendrites. This runs counter to the conventional belief that input synapses are uniformly distributed over the entire

length of SAC dendrites [Famiglietti(1991)]. The unreliability of inferring contact from co-stratification is illustrated by numerous examples of SAC dendrites that pass through BC axonal arbors without making any contact at all (Extended Data Fig. 8).

3.4 Model of direction selectivity

Above we mentioned that BC2 lags BC3a in visual response. There is another important difference: BC3a responds more transiently to step changes in illumination, while BC2 exhibits more sustained responses. The implications of the sustained-transient distinction for DS can be understood using a mathematical model. The activity of a retinal neuron is often approximated as a linear spatiotemporal filtering of the visual stimulus followed by a nonlinearity [Berry and Meister(1998), Baccus and Meister(2002)]. Such a "linear-nonlinear" model for the output $O(t)$ of the SAC dendrite can be written as

$$O(t) = \left[\int dx dt' \, W(x, t - t') I(x, t') \right]^+ \tag{3.1}$$

For simplicity, the dendrite and visual stimulus $I(x, t)$ are restricted to a single spatial dimension x, and the nonlinearity is a half-wave rectification, $[z]^+ = \max\{z, 0\}$. We interpret the integral in Eq. (3.1) as the summed input from the BCs presynaptic to the SAC. The nonlinearity could arise from various biophysical mechanisms, such as synaptic transmission from SACs to other neurons. The spatiotemporal filter $W(x, t)$ is a sum of two functions,

$$W(x, t) = U_s(x) v_s(t) + U_t(x) v_t(t) \tag{3.2}$$

corresponding to contributions from BC2 and BC3a. The sustained temporal filter $v_s(t)$ is monophasic, while the transient filter $v_t(t)$ is biphasic (Fig. 6a). The spatial filter $U_s(x)$ represents the entire set of all BC2 inputs to the dendrite, and can be estimated from the BC2 contact area graph in Figure 4d. Similarly, $U_t(x)$ can be estimated from the BC3a contact area graph. The two spatial filters are displaced relative to each other (Fig. 6a), because BC3a tends to contact SAC dendrites at more distal locations than BC2.

It is well known that direction selectivity (DS) can be generated by a model like Eqs. (3.1) and (3.2), which is based on the sum of two space-time separable filters [Watson and Ahumada(1985), Adelson and Bergen(1985)]. This is illustrated by Fig. 6 using the fact that the convolution in Eq. (3.1) is equivalent to "sliding" the spatiotemporal filter W in time over the stimulus I, and computing the overlap at each time. The filter $W(x, t)$ is oriented in space-time (Fig. 6a), and so also is a moving stimulus $I(x, t)$ (Fig. 6g,h). The overlap with a rightward-moving stimulus (Fig. 6h) is greater than for a leftward one (Fig. 6g), so the model is DS, and rightward is the preferred direction.

How is DS affected by the biphasic shape of the transient temporal filter, $v_t(t)$? If we remove the negative lobe (Fig. 6c), then $v_t(t)$ will become monophasic like $v_s(t)$ and their relation closer to a simple time lag (Fig. 6d). We will refer to this model as a "Reichardt detector," in honor of the pioneering researcher Werner Reichardt, although it more closely resembles a subunit of his model [Reichardt(1961)]. On the other hand,

removing the positive lobe of $v_t(t)$ makes it monophasic but with inverted sign relative to the sustained filter (Fig. 6e). The result (Fig. 6f) resembles a DS model originally proposed by Barlow and Levick [Barlow and Levick(1965)].

Both modified models (Figs. 6d,f) exhibit DS. In the Reichardt detector, the inputs from the two arms enhance each other for motion in the preferred direction. In the Barlow-Levick detector, the two inputs cancel each other for motion in the null direction. Since our sustained-transient model (Fig. 6b) employs both mechanisms, it should exhibit more DS than either detector. Our model is related to versions of the Reichardt detector with low-pass and high-pass filters on the two arms [Borst et al.(2003)Borst, Reisenman, and Haag].

In the original Barlow-Levick model, the negative filter corresponded to synaptic inhibition. Since BCs are believed to be excitatory, negative BC input in our model represents a reduction of excitation relative to the resting level, rather than true inhibition. Signaling by reduced excitation may be possible, at least for low contrast stimuli, as BC ribbon synapses may have a significant resting rate of transmitter release [Lagnado et al.(1996)Lagnado, Gomis, and Job].

The model of Eqs. (3.1) and (3.2) is a useful starting point for many theoretical investigations that are outside the scope of this article. For example, DS dependences on the spatial and temporal frequency of a sinusoidal traveling wave stimulus are calculated in the Supplementary Equations, and DS dependence on stimulus speed is graphed in Extended Data Figure 9.

3.5 Discussion

In our DS model, SAC dendrites are wired to BC types with different time lags. A previous model did not distinguish between BC types, and instead relied on the time lag of signal conduction within the SAC dendrite itself [Tukker et al.(2004)Tukker, Taylor, and Smith] (Fig. 1d). Like most other amacrine cells, SACs lack an axon; their output synapses are found in the distal zones of their dendrites [Famiglietti(1991)] (Fig. 1a, inset). Due to dendritic conduction delay, proximal BC inputs should take longer to reach the output synapses than distal BC inputs (Fig. 1d). Therefore this time lag is also consistent with the empirical finding of an outward preferred direction. To summarize the novelty of our hypothesis, we place the time lag before BC-SAC synapses, whereas the previous model places it after BC-SAC synapses.

The postsynaptic delay model has a major weakness. If dendritic conduction were the only source of time lag, the somatic voltage would exhibit DS with an inward preferred direction, but this is inconsistent with intracellular recordings [Euler et al.(2002)Euler, Detwiler, and Denk] (Fig. 1e). In contrast, the presynaptic delay model is compatible with approximating an SAC dendrite as isopotential (Fig. 1c), so preferred direction is predicted to be independent of the location of the voltage measurement, consistent with empirical data [Euler et al.(2002)Euler, Detwiler, and Denk]. It may also be possible to make the postsynaptic delay model consistent with experiments by adding active dendritic conductances [Hausselt et al.(2007)Hausselt, Euler, Detwiler, and Denk].

The presynaptic and postsynaptic delay models are not mutually exclusive. If they

work together, passive cable theory suggests that presynaptic delay dominates, because estimated postsynaptic delay is much shorter than the time lag between BC2 and BC3a (Supplementary Equations). Can we gauge the relative importance of the delays empirically rather than theoretically? One way would be intracellular recording at the SAC soma of responses to visual stimulation at various dendritic locations. If postsynaptic delay dominates, then response latency will grow with distance of the visual stimulus from the soma. If presynaptic delay dominates, then distal stimulation will evoke somatic responses with shorter latency than proximal stimulation. This prediction may seem counterintuitive, but is an obvious outcome of our model.

Many other models of DS emergence in SACs invoke inhibition as well as excitation [Borg-Graham and Grzywacz(1992), Gavrikov et al.(2003)Gavrikov, Dmitriev, Keyser, and Mangel, Münch and Werblin(2006), Lee and Zhou(2006)]. We have focused on excitatory mechanisms, as blocking inhibition does not abolish DS [Euler et al.(2002)Euler, Detwiler, and Denk]. However, inhibition may have the effect of enhancing DS, and its role should be investigated further.

This work focused on Off BC-SAC circuitry. An analogous sustained-transient distinction can also be made for On BC types [Baden et al.(2013)Baden, Berens, Bethge, and Euler, Borghuis et al.(2013)Borghuis, Marvin, Looger, and Demb]. It remains to be seen whether their connectivity with On SACs depends on distance from the soma. If this turns out to be the case, then the model of Figure 6 could serve as a general theory of motion detection by both On and Off SACs. The model filter of Figure 6a also resembles the spatiotemporal receptive field of the J type of ganglion cell (Fig. 3b of Ref. [Kim et al.(2008)Kim, Zhang, Yamagata, Meister, and Sanes]).

Neural activity imaging [Maisak et al.(2013)Maisak, Haag, Ammer, Serbe, Meier, Leonhardt, Schilling, B and connectomic analysis [Takemura et al.(2013)Takemura, Bharioke, Lu, Nern, Vitaladevuni, Rivlin, Katz have recently identified a plausible candidate for the site of DS emergence in the fly visual system. If our theory is correct, then the analogies between insect and mammalian motion detection [Borst and Euler(2011)] are more far-reaching than previously suspected, with fly T4 and T5 cells corresponding to On and Off SAC dendrites in both connectivity and function.

A glimmer of space-time wiring specificity can even be seen in the structure of the SAC itself. Since BC types with different time lags arborize at different IPL depths, IPL depth can be regarded as a time axis. Therefore, the slight tilt of the SAC dendrites in the IPL (Fig. 5a) could be related to the orientation of the SAC receptive field in space-time (Fig. 6a). However, dendritic tilt alone is not sufficient to predict our model, as co-stratification sometimes fails to predict contact (Figs. 4d, 5b). For example, co-stratification predicts strong BC4 connectivity to distal SAC dendrites. This would favor an inward preferred direction, contrary to what is observed, because BC2 leads (not lags) BC4 in visual responses [Baden et al.(2013)Baden, Berens, Bethge, and Euler].

The idea that contact (or connectivity) can be inferred from co-stratification is sometimes known as Peters' Rule [Braitenberg and Schüz(1998)], and has also been applied to estimate neocortical connectivity [Kalisman et al.(2003)Kalisman, Silberberg, and Markram, Binzegger et al.(2004)Binzegger, Douglas, and Martin, Stepanyants and Chklovskii(2005)]. The present work shows that fairly subtle violations of Peters' Rule may be important

for visual function. Previous research suggests that On-Off direction selective ganglion cells (DSGCs) inherit their DS from SAC inputs due to a strong violation of Peters' Rule [Fried et al.(2002)Fried, Münch, and Werblin, Yonehara et al.(2010)Yonehara, Balint, Noda, Nagel, Bamberg Wei et al.(2010)Wei, Hamby, Zhou, and Feller, Briggman et al.(2011)Briggman, Helmstaedter, and Denk].

Our findings were made possible by using AI to reduce the amount of human effort required for 3D reconstruction of neurons. Even after the labor savings, our research required great human effort from a handful of paid workers in the lab and a large number of volunteers through EyeWire. Our experiences do not support claims that the "wisdom of the crowd" should replace experts [Surowiecki(2005)]. Instead, EyeWire depends on cooperation between lab experts and online amateurs (Methods). Furthermore, some amateurs developed remarkable expertise and were promoted to increasingly sophisticated roles within the EyeWire community (Supplementary Notes). We believe that crowd wisdom requires amplifying the expert voices within the crowd, and also empowering individuals to become experts. Fortunately, such goals are well-matched to the game format.

The EyeWire AI was based on a deep convolutional network [Turaga et al.(2009)Turaga, Briggman, Helms Turaga et al.(2010)Turaga, Murray, Jain, Roth, Helmstaedter, Briggman, Denk, and Seung]. Similar networks have been successfully applied to serial EM images obtained using conventional staining techniques that mark intracellular organelles [Ciresan et al.(2012)Ciresan, Giusti, Schmidl Extending EyeWire to such images, in which synapses are clearly visible, would enable a true connection analysis that goes beyond the contact and co-stratification analyses employed here.

Our work demonstrates that reconstructing a neural circuit can provide surprising insights into its function. Much more will be learned as reconstruction speed grows. The combination of crowd and artificial intelligence promises a continuous upward path of improvement, as human input from the crowd is not only useful for generating neuroscience discoveries, but also for making the AI more capable through machine learning.

3.6 Methods summary

A convolutional network (CN) was trained to detect neural boundaries via the MALIS procedure[Turaga et al.(2009)Turaga, Briggman, Helmstaedter, Denk, and Seung] and CNPKG (https://github.com/srinituraga/cnpkg/), which is based on Cortical Network Simulator [Mutch et al.(2010)Mutch, Knoblich, and Poggio]. The CN was applied to the e2198 dataset, which was then segmented into supervoxels by a modified version of the watershed algorithm. Paid workers and volunteer EyeWirers reconstructed neurons in 3D by assembling supervoxels. The retina was computationally flattened, reconstructed neurons were classified by their structural properties, and contact and co-stratification were analyzed by custom MATLAB and C++ code.

3.7 Methods from Supp

Machine learning   The boundaries between neurons in subvolumes of the e2198 and e2006 datasets were manually traced. Using this as ground truth, a convolutional network (CN) was trained to detect boundaries between neurons using the MALIS method [Turaga et al.(2009)Turaga, Briggman, Helmstaedter, Denk, and Seung]. The CN had the same architecture as one used previously [Helmstaedter et al.(2013)Helmstaedter, Briggman, Turaga, Ja and produced as output an affinity graph connecting nearest neighbor voxels [Turaga et al.(2010)Turaga, Mu Any subvolume of e2198 could be oversegmented by applying a modified watershed algorithm to the appropriate subgraph. The regions of the oversegmentation will be called supervoxels.

Reconstruction by workers   A team of part-time workers, numbering about half a dozen at any given time, also reconstructed neurons using a more sophisticated version of the EyeWire interface. Workers were hired based on an interview and a short test of software use passed by 3/4 of the applicants. They were trained for 40 to 50 hours before generating reconstructions used for research. Their skills typically improved for months or even years after the initial training period, and were superior to those of professional neuroscientists without reconstruction experience.

As with EyeWire, the task of reconstructing an entire neuron was divided into subtasks, each of which involved reconstructing the neuron within a subvolume starting from a supervoxel "seed." However, the subvolumes were roughly 100 times larger than EyeWire cubes, and only two workers were assigned to each subvolume. In the first stage of error correction, disagreements were detected by computer, and resolved by one of the two workers, or a third worker. The third occasionally detected and corrected errors that were not disagreements between the first two. Most disagreements were the result of careless errors, and were easily resolved. More rarely, there were disagreements caused by fundamental ambiguities in the image. These locations were noted for later examination with more contextual information, as described below.

In the second stage of error correction, 3D reconstructions of entire neurons were assembled from multiple subvolumes and inspected by one of the authors (J.S.K.). Suspicious branches or terminations, as well as overlaps between reconstructions of different neurons were detected. The original image was reexamined at these locations to check for errors. The process was repeated until no further errors could be detected. The F-score (Figure 2b) between the reconstructions before and after the second stage was 0.99 for SACs and 0.98 for BCs. Some errors may still remain, but it is likely that correcting them would have similarly little effect.

Reconstruction by EyeWirers   Even before the learning in normal gameplay illustrated by Figure 2d, all EyeWirers are required to go through a training session immediately after registering for the site. This consists of a sequence of tutorial cubes, each of which was previously colored by an expert (Supplementary Figure 6). Each cube teaches through instructions and per-click feedback about accuracy based on comparing the EyeWirer's

selections with those of the expert. After submitting a tutorial cube, the EyeWirer is given a chance to view mistakes.

Accuracy is monitored on a weekly basis by computing the precision and recall of each EyeWirer with respect to the truth, defined as neuron reconstructions based on EyeWire consensus followed by GrimReaper corrections. Less accurate EyeWirers are given less weight in the vote, which appears to improve the overall accuracy of the system.

Players' daily, weekly, and monthly scores are publicly displayed on a leaderboard (Supplementary Figure 7, right), motivating players to excel through competition. Players communicate with each other through online "chat" (Supplementary Figure 7, left) and discussion forums.

A "beta test" version of EyeWire was deployed in February 2012, and attracted a small group of users, who helped guide software development. After the official launch in December 2012, EyeWire was successful at reconstructing ganglion cells, but did not work well for reconstructing the more difficult SACs. In March 2013, EyeWirers were invited to the "Starburst Challenge," a sequence of tutorial cubes drawn from SACs. Those who passed with sufficient accuracy were an elite group allowed to reconstruct SACs (Supplementary Information).

Some SACs were reconstructed twice, once by workers and once by EyeWire.

Reconstruction of Off SACs Off SACs were reconstructed by (1) forward tracing from the soma to dendritic tips and (2) backward tracing from varicosities on candidate SAC dendrites to the soma. In the forward method, a candidate SAC soma was identified as a supervoxel with a characteristic pattern of dendritic stubs bearing spiny protrusions. By the time reconstruction progressed to approximately half of the average SAC radius, an Off SAC could be conclusively recognized by its starburst shape and narrow stratification at the appropriate IPL depth. More than 90% of candidates turned out to be SACs.

In the backward method, we located a thin dendrite with varicosities at the appropriate IPL depth. This was reconstructed back to the soma, and then the rest of the dendrites were reconstructed from the soma to the tips. The cell could be discarded at any point during this process, if its dendrites escaped from the appropriate IPL depth or failed to exhibit the proper morphological characteristics. Less than 25% of initial candidates ended up confirmed as SACs.

In total, 79 Off SACs were reconstructed, 39 by forward tracing and 52 by backward tracing. After candidates were identified by one of the authors (J.S.K.), reconstructions were performed by lab workers (59 cells) or by EyeWirers (29 cells). Overlapping numbers (12 for forward/backward, 9 for workers/EyeWirers) mean the combination of the two.

Reconstruction of Off BCs Because only part of the inner nuclear layer (INL) was encompassed in e2198, the somata of Off bipolar cells (BCs) were generally outside the dataset. Therefore we searched the INL for candidate BC axons traveling between the somata, and traced them into the INL. Those that arborized in the Off region of the INL were further reconstructed. Cells that violated known BC structures were identified as amacrine cells and discarded [Helmstaedter et al.(2013)Helmstaedter, Briggman, Turaga, Jain, Seung, and]

BC axons were difficult to reconstruct due to poor staining, and their highly irregular shapes. They could not be accurately reconstructed (either by online volunteers or lab experts) within the 256^3 cubes of EyeWire, which were too small to provide sufficient spatial context. Therefore BCs were reconstructed only by lab workers using the large subvolumes mentioned above.

Coordinate system   For more precise quantification of structural properties, a new coordinate system was defined by applying a nonlinear transformation to reconstructed neurons so as to flatten the IPL and make it perpendicular to one of the coordinate axes. The nonlinear transformation was found by the following steps. First a global planar approximation to the Off SAC surface was computed. Then the centroid of all the SACs was projected onto this global plane to define the origin of the coordinate system. The projection was along the coordinate axis of the e2198 volume closest in direction to the light axis.

To correct for curvature, an azimuthal equidistant projection of the Off SAC surface onto the global plane was made about the origin . Then local planar approximations to the SAC surface were computed in the neighborhoods of every node in a triangular lattice. At each point in a triangle, the SAC surface was approximated by computing the mean of the planar approximations (as quaternions with yaw constrained to be zero) for the triangle's vertices, weighted by distance of the point from the vertices.

The Off SACs were defined as 32% IPL depth. We also reconstructed a few On SACs, and defined them as 62%. These choices placed the edge of the INL at 0%. Structural properties of all cells were computed based on the locations of their surface voxels after transformation into the new coordinates. All dimensions are uncorrected for tissue shrinkage, which was previously estimated at 14% by comparison of two-photon and serial EM images [?].

Classification of Off bipolar cells   BC stratification profiles were computed by dividing surface voxels into 100 bins spanning 0 to 100% IPL depth. Classification into cell types was done by using methods similar to those described previously [Helmstaedter et al.(2013)Helmstaedter, Bri The BCs were split into shallow (BC1/2) and deep (BC1/2) clusters using the 75th percentile depth of the stratification profile. The BC1/2 cluster was further subdivided by stratification width, defined as the difference between 75th and 25th percentile depths. The wider cluster was identified as BC2 and the narrower cluster as BC1, based on a molecular classification showing that BC2 has more cells per square millimeter than BC1 [Wässle et al.(2009)Wässle, Puller, Müller, and Haverkamp]. This correspondence between structural and molecular classifications is the opposite of a previous report [Helmstaedter et al.(2013)Helmstaedter, Briggman, Turaga, Jain, Seung, and Denk]. The discrepancy may be due to methodological differences, such as computing stratification profiles based on surface voxels versus skeletons. The BC3/4 cluster was subdivided into BC4 and BC3 by the 10th percentile depth, because the molecularly defined BC4 stratifies closer to the INL [Wässle et al.(2009)Wässle, Puller, Müller, and Haverkamp]. Finally, BC3 was subdivided into BC3a and BC3b based on axonal arbor volume, with

BC3a having the larger axonal volume. Supplementary Figure xxx shows that each of the above subdivision steps was based on a feature with a roughly bimodal histogram.

The result still contained a small number of classification errors, as adjacent BCs of the same type overlapped enough to violate the mosaic property. Corrections were made by an automatic algorithm that greedily swapped cells from one cluster to another such that the total overlap between convex hulls of cells of a given type was minimized. Two swaps were vetoed by an expert (J.S.K) on the basis of morphological features. In all, six cells were swapped within BC1/2 and 13 within BC3/4. In the final classification, 41, 56, 29, 35, and 34 BCs were identified as types 1, 2, 3a, 3b, and 4, respectively (Supplementary Figure 2a-e, Supplementary Table 1). A few cells that violated the mosaic of all types and had irregular stratification profiles were discarded as possible reconstruction errors or amacrine cells.

Contact analysis Edges of the affinity graph connecting BC with SAC voxels were defined as BC-SAC contact edges. For each pair, the sum of the edges yielded an estimate of contact area. The Euclidean distance separating each BC-SAC pair was computed after projecting their centers onto the SAC plane. Centers of SAC somata were manually annotated, and centers of BC arbors were computed as the centroids of their surface voxels. The pairs were binned by distance of the BC from the SAC soma. For every pair in a bin, the fraction of SAC surface area devoted to BC-SAC contact within the convex hull of the BC was computed as the ratio of BC-SAC contact edges to SAC surface edges within the convex hull. The latter was estimated by the number of SAC surface voxels multiplied by a geometric conversion factor of 1.4 SAC surface edges per surface voxel. (This factor was estimated by dividing the total number of SAC surface edges by the total number of SAC surface voxels in the volume.) BC-SAC pairs with fewer than 10,000 SAC surface voxels inside the hull were excluded from the computation to reduce the effect of fluctuations. The ratios for BCs of the same type were averaged for each distance bin and multiplied by a mosaic overlap factor to yield the values in Figure 4d. The mosaic overlap factor represents the extent to which neighboring convex hulls overlap one another, which varies by cell type. This factor was computed by dividing the sum of the hull areas for each cell by the area of the union of hulls for each cell type.

In instances where edges in the affinity graph are converted to area in μm^2, the conversion factor of $291.5\mu m^2$ per edge is used. This factor estimates the real surface area of the cell given the different possible orientations of edges and effects from pixelization.

Co-stratification analysis All SAC surface voxels were binned by distance from the soma center in the SAC plane. Within each bin, the stratification profile was computed as for the BCs. The quartiles (median and 25th and 75th percentiles) are graphed in Figure 5a. The prediction of contact from co-stratification is based on the following formalism.

We define the arbor density $\rho_a(\vec{r})$ as the surface area per unit volume at location $\vec{r}$ of a type a cell with soma centered at the origin. Its integral $\int d^3r\, \rho_a(\vec{r})$ is the total surface area of the arbor. We assume that the contact density received by one cell of type a from

all cells of type b is equal to

$$c_{ab}(\vec{r}) = \rho_a(\vec{r}) \sum_i \rho_b(\vec{r} - \vec{r}_{bi}) \qquad (3.3)$$

The sum over the b mosaic can be approximated by a function that is independent of x and y,

$$\sum_i \rho_b(\vec{r} - \vec{r}_{bi}) \approx \sigma_b s_b(z) \qquad (3.4)$$

where σ_b is the number of type b neurons per retinal area and

$$s_b(z) = \int dx dy \, \rho_b(x, y, z) \qquad (3.5)$$

is the stratification profile of a cell of type b. The SAC arbor density is assumed radially symmetric, $\rho_{SAC}(\vec{r}) = \rho_{SAC}\left(\sqrt{x^2 + y^2}, z\right)$, where ϕ can be regarded (up to normalization) as the SAC stratification profile as a function of distance $r = \sqrt{x^2 + y^2}$ from the SAC soma. Integrating the contact density (3.3) and normalizing yields the fraction $\phi_b(r)$ of SAC area contacted by cell type b as a function of r,

$$\phi_b(r) = \sigma_b \frac{\int dz \, \rho_{SAC}(r, z) s_b(z)}{\int dz \, \rho_{SAC}(r, z)} \qquad (3.6)$$

Mathematical model of the BC-SAC circuit The output $O(t)$ of a SAC dendrite is modeled as

$$O(t) = g\left(\sum_{i=1}^n c_i f_i \left(\int dx dt' w_i(x, t - t') I(x, t')\right)\right) \qquad (3.7)$$

The dendrite and the visual stimulus $I(x, t)$ are restricted for simplicity to a single spatial dimension x. The ith BC filters the visual stimulus with $w_i(x, t)$, and the result is passed through the nonlinear function f_i. The contributions from the BCs are weighted by the $c_i < 0$, summed, and passed through a nonlinear function g.

Suppose that $f_i(z) = [z + b_i]^+$ with $b_i > 0$ corresponding to spontaneous output in the absence of visual stimulation. Then the BC output nonlinearity can be neglected for visual stimuli with sufficiently small amplitude. Also suppose that $g(z) = [z - a]^+$, where $a > 0$ corresponds to a threshold for SAC response, or some source of spontaneous inhibitory input. Then Eq. (3.7) simplifies to

$$O(t) = \left[\int dx dt' \sum_{i=1}^n c_i w_i(x, t - t') I(x, t') + \sum_i b_i c_i - a\right]^+ \qquad (3.8)$$

Now assume that each spatiotemporal filter is separable, $w_i(x, t) \approx u_i(x) v_i(t)$, and that each temporal filter is either sustained or transient, $v_s(t)$ or $v_t(t)$. Then

$$\sum_i c_i w_i(x, t) \approx U_s(x) v_s(t) + U_t(x) v_t(t)$$

where $U_s(x) = \sum_{i \in S} c_i u_i(x)$ and $U_t(x) = \sum_{i \in T} c_i u_i(x)$ are the weighted sums of spatial filters over the sustained and transient sets of BCs. Finally, Eq. (3.8) reduces to Eq. (**??**) if $a = \sum_i b_i c_i$.

If the visual stimulus is a sinusoidal traveling wave, $I(x, t) = \cos(kx - \omega t)$, then the integral in Eq. (**??**) yields a sine wave given by the real part of

$$[\tilde{u}_s(k)\tilde{v}_s(\omega) + \tilde{u}_t(k)\tilde{v}_t(\omega)] \, e^{-i\omega t} \;\; = \;\; \tilde{u}_s(k)\tilde{v}_s(\omega) \left[1 - i\omega\tau e^{ik\Delta x}\right] e^{-i\omega t}$$

where $\tilde{u}_s(k) = \int dx \, e^{ikx} u_s(x)$ and other Fourier transforms are defined similarly. The amplitude of the sine wave defines the peak and time-averaged response of Eq. (**??**):

$$
\begin{aligned}
A(k, \omega) &= |\tilde{u}_s(k)| \, |\tilde{v}_s(\omega)| \left|1 - i\omega\tau e^{ik\Delta x}\right| \\
&= |\tilde{u}_s(k)| \, |\tilde{v}_s(\omega)| \sqrt{1 + 2\omega\tau \sin k\Delta x + (\omega\tau)^2}
\end{aligned}
$$

The term linear in ω is the DS component of the response. Assuming $\omega > 0$ and $\Delta x > 0$ without loss of generality, the preferred direction (PD) is rightward for spatial frequencies satisfying $|k\Delta x| < \pi$. Outside this range, spatial aliasing can cause the PD to reverse. The direction selectivity index (DSI) is

$$DSI \;\; = \;\; \frac{PD - ND}{PD} = 1 - \sqrt{\frac{1 - 2\omega\tau \, |\sin k\Delta x| + (\omega\tau)^2}{1 + 2\omega\tau \, |\sin k\Delta x| + (\omega\tau)^2}}$$

which can be rewritten as Eq. (**??**) in the main text. This is a periodic function of k, because the DSI is a ratio of responses. The responses themselves will typically vanish for large k, due to the spatial filtering, but the DSI is independent of the filter functions. According to the second line, $0 \leq DSI \leq 1$. The third line is maximized for any fixed ω when $k\Delta x = \pi/2$. This means that an optimal wavelength for the stimulus is $\lambda = 4\Delta x$. Then

$$DSI = 1 - \frac{1 - \omega\tau}{1 + \omega\tau}$$

which in turn is maximized when $\omega\tau = 1$.

4 An Analagous Model in the On SAC

The starburst amacrine cell (SAC) is a key player in retinal computation of the direction
of a moving stimulus. Ablation of SACs impairs the optokinetic reflex, a behavior that de-
pends on computation of visual motion [Yoshida et al.(2001)Yoshida, Watanabe, Ishikane, Tachibana, Pasta
Amthor et al.(2002)Amthor, T, and Dmitrieva]. Both ablation [Yoshida et al.(2001)Yoshida, Watanabe, Ish
Amthor et al.(2002)Amthor, T, and Dmitrieva] and reversible inactivation [Vlasits et al.(2014)Vlasits, Bos,
of SACs reduce direction selective (DS) responses in ganglion cells, which receive synaptic
input from SACs. SAC dendrites are preferentially activated by visual stimuli that move
outward from the soma to the dendritic tips [Euler et al.(2002)Euler, Detwiler, and Denk,
Lee and Zhou(2006), Hausselt et al.(2007)Hausselt, Euler, Detwiler, and Denk].

The proposed mechanisms for DS of SAC dendrites fall into several categories. Accord-
ing to inhibitory cellular hypotheses, dendritic biophysics causes inhibitory input to SACs
to have effects that depend on dendritic location [Borg-Graham and Grzywacz(1992),
Gavrikov et al.(2003)Gavrikov, Dmitriev, Keyser, and Mangel]. In inhibitory circuit hy-
potheses, GABAergic synaptic connectivity between SAC dendrites depends on the differ-
ence between their preferred directions [Lee and Zhou(2006), Münch and Werblin(2006)].
In excitatory cellular hypotheses, SAC biophysics causes excitatory input to SACs to have
effects that depend on dendritic location [Tukker et al.(2004)Tukker, Taylor, and Smith,
Hausselt et al.(2007)Hausselt, Euler, Detwiler, and Denk, Oesch and Taylor(2010)].

Recently we proposed a novel excitatory circuit hypothesis based on specificity of wiring
between bipolar cells (BCs) and SACs. The proposal was based on anatomical evidence
that sustained and transient BC types are connected to SACs at locations that are near
and far from the SAC soma, respectively [Kim et al.(2014)Kim, Greene, Zlateski, Lee, Richardson, Turaga,
Such "space-time wiring specificity" could make the BC-SAC circuit function as a correlation-
type motion detector [Borst and Euler(2011)], and is consistent with the observed out-
ward preferred direction of SAC dendrites.

Like many other retinal neurons, the SAC comes in both On and Off types. The
On SAC resembles a reflection of the Off SAC across a plane through the middle of
the inner plexiform layer (IPL) (Fig. 1B, D). Probably due to this striking symmetry,
DS and its mechanisms are often assumed to be similar between On and Off SACs.
This remains merely an assumption as published studies of SACs were typically re-
stricted to a single type. Physiological studies of DS were carried out for On SACs
[Euler et al.(2002)Euler, Detwiler, and Denk, Lee and Zhou(2006), Hausselt et al.(2007)Hausselt, Euler, De
while our anatomical study of BC-SAC wiring specificity was carried out for Off SACs
[Kim et al.(2014)Kim, Greene, Zlateski, Lee, Richardson, Turaga, Purcaro, Balkam, Robinson, Behabadi, G
Here we find evidence that the On BC-SAC circuit possesses a space-time wiring speci-
ficity analogous to that shown previously for the Off BC-SAC circuit. We reconstructed
a large set of On BCs and On SACs from e2198, a dataset of mouse retinal images from se-

rial block-face scanning electron microscopy [Briggman et al.(2011)Briggman, Helmstaedter, and Denk]. Based on the resulting high-resolution information about the anatomy of single cells, we have succeeded in subdividing BC5 into three types that we call BC5t, BC5i, and BC5o. This finding confirms a speculation of [Helmstaedter et al.(2013)Helmstaedter, Briggman, Turaga, Jain, Seu who were previously able to distinguish just two BC5 types, but predicted the existence of more. Our definition of a third BC5 type increases the total count of cone BC types to 13.

Contact analysis is consistent with a wiring diagram in which BC7 prefers to synapse closer to the On SAC soma, and BC5 prefers to synapse farther from the soma (Fig. 1C). Among the BC5 types, synaptic input from BC5o is likely to be less than from BC5t and BC5i.

Most of the available evidence suggests that transient BC types generally arborize near the IPL center, and sustained BC types near the IPL edges [Baden et al.(2013)Baden, Berens, Bethge, and E Borghuis et al.(2013)Borghuis, Marvin, Looger, and Demb]. (But see [Ichinose et al.(2014)Ichinose, Fyk-Ko for a divergent view.) Combined with the standard division of the IPL into On and Off sublamina, this yields four sublayers: On-sustained, On-transient, Off-transient, and Off-sustained (Fig. 1B). Based on this IPL organization, it is likely that BC7 is sustained and BC5 is transient. If this is the case, then On BC-SAC wiring is analogous to Off BC-SAC wiring.

4.1 Results

a

4.2 Aligning cells to a common coordinate system

The cell bodies of On and Off SACs are in the GCL and INL respectively, on oppo-site sides of the IPL (Fig. 1B, D). The reconstructions include 156 SACs (77 On and 79 Off, Fig. 1E), which we estimate is more than half of the SACs in e2198 (Experi-mental Procedures). The diameter of the SAC arbor is much larger than the spacing between cell bodies (Fig. 1E), so the arbors of adjacent SACs are highly overlapping. The reconstructions also include 271 On BC axons, coming close to complete cover-age of all BCs in a subregion of e2198 roughly $(0.1 \text{ mm})^2$ in area (Fig. 1E). BC ax-ons are much smaller than SAC arbors (Fig. 1E). The reconstructions of On SACs and BCs are new, while the Off SACs were reconstructed for a previous publication [Kim et al.(2014)Kim, Greene, Zlateski, Lee, Richardson, Turaga, Purcaro, Balkam, Robinson, Behabadi, G For classification of retinal cell types, we relied heavily on the stratification profile, de-fined as the distribution of a cell's surface area over the depth of the IPL. It is standard to use On and Off SACs as landmarks to define IPL depth. Since the IPL has curvature and variations in thickness (Fig. 2A), we computationally flattened the retina by transforming the On and Off SACs into parallel planes (Fig. 2B). This type of coordinate transfor-mation improves the accuracy of stratification profiles, and has previously been applied in light microscopic anatomy [Manookin et al.(2008)Manookin, Beaudoin, Ernst, Flagel, and Demb,

Siegert et al.(2009)Siegert, Scherf, Del Punta, Didkovsky, Heintz, and Roska, Sümbül et al.(2014)Sümbül, S
Average On and Off SAC stratification profiles became narrower after the transformation
(Fig. 2C).

[Famiglietti(1983)] divided SAC dendrites into proximal, intermediate, and distal zones.
The median stratification depth of SAC dendrites varies strongly in the proximal zone,
weakly in the intermediate zone, and is roughly constant in the distal zone (Fig. 2D).

In studies of rabbit retina, [Famiglietti(1991)] reported that presynaptic boutons are
confined almost exclusively to the distal zone, while synaptic inputs from bipolar and
amacrine cells are found in all zones. We found that the fraction of On SAC sur-
face in contact with BCs is smaller in the distal zone (Fig. 2E), suggesting that BC
synapses have some preference for the proximal and intermediate zones of SAC dendrites.
We previously reported a similar dependence for Off SACs (Extended Data Fig. 7 of
[Kim et al.(2014)Kim, Greene, Zlateski, Lee, Richardson, Turaga, Purcaro, Balkam, Robinson, Behabadi, (
the effect is stronger for On SACs (Fig. 2E).

4.3 Subdivision of BC5 into three cell types

Mouse BCs were originally classified into nine cone types (BC1 through BC9) and one rod
type based on light microscopic anatomy [Ghosh et al.(2004)Ghosh, Bujan, Haverkamp, Feigenspan, and Wä
Later on, BC3 was subdivided into BC3a and BC3b based on molecular differences
[Wässle et al.(2009)Wässle, Puller, Müller, and Haverkamp]. Then electron microscopic
anatomy was used to distinguish BC3a and BC3b, divide BC5 into two types, and discover
a new XBC type [Helmstaedter et al.(2013)Helmstaedter, Briggman, Turaga, Jain, Seung, and Denk].

We revisited the classification of On BCs using the e2198 reconstructions (Experimen-
tal Procedures and Fig. S1). As shown in the gallery of example cells (Fig. 3A, B), On
BC axons are found in half the depth of the IPL, closer to the GCL than the INL. Our On
BC types correspond to those defined previously, with good agreement regarding densities
(compare Fig. 3D with Fig. 1E inset of [Helmstaedter et al.(2013)Helmstaedter, Briggman, Turaga, Jain, Se
The novelty is the subdivision of BC5 into three types called BC5t, BC5i, and BC5o.
The three types stratify at similar depths (Figs. 3A,C), which is why they were originally
grouped into a single Type 5 [Ghosh et al.(2004)Ghosh, Bujan, Haverkamp, Feigenspan, and Wässle].
Nevertheless, it is possible to differentiate between the types based on subtle differences
between their stratification profiles. BC5-inner ("BC5i") stratifies slightly more towards
the inner retina than the other types (Figs. 3A,C and S1B). BC5-thick ("BC5t") is more
thickly stratified than BC5-outer ("BC5o"), as shown in Figs. 3A,C and S1D. The strat-
ification profile of BC5t is weakly bimodal (Fig. 3C), but this property was not used for
the classification.

We are confident of our three-way division of BC5 based on stratification (Experimental
Procedures and Fig. S1), because the axonal arbors of each cluster end up roughly tiling
the retina with little overlap (Fig. 3E, F, G). This "tiling principle" is thought to be a
defining characteristic of a true bipolar cell type [Wässle et al.(2009)Wässle, Puller, Müller, and Haverkamp]
On the other hand, when BC5 cells are divided into just two clusters, it is impossible to
avoid many collisions between highly overlapping axonal arbors (Fig. 4E).

Only a few violations of the tiling principle are evident in Figs. 3E, F, and G. One possibility is that the tiling principle holds only approximately, and that the violations are a form of biological "noise." Another possibility is that the violations result from errors in our classification procedure. Therefore, we generated a "corrected" classification by swapping a few cells between types (Experimental Procedures). The number of swaps is relatively small (Table S1). The "type gallery" of Fig. S3 exhibits our final classification after swapping. The corrected classification was the basis of subsequent analysis of BC-SAC wiring, but our results are qualitatively unchanged even if the uncorrected classification is used.

4.4 Defining bipolar cell types based on contact

Only if the stratification profiles of two cells overlap is there potential for contact between the cells, and hence potential for synaptic connections. In other words, stratification constrains retinal connectivity [Masland(2004)]. It follows that cell types defined using stratification are likely to end up having functional significance, assuming that the connectivity of a cell is closely related to its function [Seung and Sümbül(2014)].

It would be more direct to define a cell type as a set of cells with similar contact or connectivity patterns [Seung(2009), Seung(2012)], rather than use stratification as a proxy for these properties. For example, the 302 neurons of *C. elegans* were divided into 118 classes, each containing neurons with similar connectivity patterns [White et al.(1986)White, Southgate, Thomson, and Brenner]. Likewise [Helmstaedter et al.(2013)Helmsta divided BC5 into classes based on patterns of contact with two ganglion cell types named "gc31-56" and "gc36-51." We decided to replicate their analysis, mainly in order to determine the correspondence between contact-based and stratification-based classifications. A secondary motivation was to examine how contact-based classification depends on the completeness of reconstruction. [Helmstaedter et al.(2013)Helmstaedter, Briggman, Turaga, Jain, Seung, an reconstructed all neurons with cell bodies contained in a $(0.1 \text{ mm})^2$ patch. This method missed ganglion cells with arbors inside the patch but cell bodies outside the patch, which is why gaps in coverage are visible in the gallery of cell types provided in the Supplementary Data of [Helmstaedter et al.(2013)Helmstaedter, Briggman, Turaga, Jain, Seung, and Denk]. Contact with missing arbors obviously cannot be quantified, hampering contact-based classification.

We were able to replicate and improve the contact-based classification by making use of a large set of ganglion cells that were reconstructed from the e2198 dataset in a parallel study to be reported elsewhere. From this set of ganglion cells, we identified 16 examples of gc31-56 and 19 examples of gc36-51 based on their distinctive stratification profiles (Figs. 4A, B). The arbors of each ganglion cell type completely cover the central region of e2198 where the bipolar cells are located, because the reconstructed ganglion cells include those with cell bodies outside the central region (Fig. S3). For each BC5 cell, we quantified the fraction of its axonal surface area in contact with gc31-56 cells, and the fraction of its axonal area in contact with gc36-51 cells. Then BC5 indeed splits nicely into two clusters based on the two contact fractions (Fig. 4C). One cluster, named "BC5A"

by [Helmstaedter et al.(2013)Helmstaedter, Briggman, Turaga, Jain, Seung, and Denk], has more contact with gc31-56. BC5A tiles with few violations (Fig. 4E) and therefore appears to be a pure cell type. BC5A corresponds almost exactly with BC5i (Fig. 4C).

The other cluster, named "BC5R" by [Helmstaedter et al.(2013)Helmstaedter, Briggman, Turaga, Jain, Se has more contact with gc36-51. Because BC5R contains many tiling violations (Fig. 4E), [Helmstaedter et al.(2013)Helmstaedter, Briggman, Turaga, Jain, Seung, and Denk] speculated that BC5R was a mixture of more than one type. Our stratification-based classification confirms their speculation by effectively dividing BC5R into BC5o and BC5t, both of which tile the retina separately.

The cleanness of the division between BC5A and BC5R is evident in a histogram of the difference between the gc31-56 and gc36-51 contact fractions, in which two well-separated clusters are evident (Fig. 4D). Note that [Helmstaedter et al.(2013)Helmstaedter, Briggman, Turaga, Jain, S labeled some of their reconstructed cells as BC5X. This name was not intended to be a type but rather indicated cells that were unclassifiable because they lacked contact with gc31-56 and gc36-51. We do not have this problem because our coverage of the ganglion cell types is more complete.

4.5 BC-SAC contact analysis

We computed contact area between SACs and BCs of each type. The absolute areas were normalized to produce an estimate of the percentage of SAC surface area covered by BCs of each type (Experimental Procedures). This contact analysis suggests that BC5t, BC5i, and BC7 are likely the dominant bipolar cell inputs to the On SAC (Fig. 5A, C). Our result is consistent with previous anatomical reconstructions [Helmstaedter et al.(2013)Helmstaedter, Briggman, Turaga, Jain, Seung, and Denk] and physiological experiments [Duan et al.(2014)Duan, Krishnaswamy, De la Huerta, and Sanes, Chen et al.(2014)Chen, Lee, Park, Looger, and Zhou], though these previous studies did not distinguish all three BC5 types. If there is BC5o input, it is likely substantially weaker than BC5t and BC5i input (Fig. 5A).

To characterize the spatial relations between contacting cells, we examined the dependence of BC-SAC contact on distance between the BC axon and the SAC soma (Fig. 5B). The absolute areas were normalized to estimate the percentage of SAC surface area covered by BCs of a given type at a particular distance from the SAC soma (Experimental Procedures). The resulting graphs show that BC7 prefers to contact On SAC dendrites near the SAC soma, whereas BC5t and BC5i prefer to contact at an intermediate distance from the soma (Fig. 5C).

One might worry that our contact analyses are sensitive to incomplete reconstruction of BCs (see Experimental Procedures and "holes" in the tilings of Figs. 3E, F, G). To avoid this problem, the results of our analyses are expressed not as absolute contact areas but instead as fractions of SAC surface area. To demonstrate robustness, we repeated our contact analyses after deleting a random subset of BC5t and BC5i cells (Fig. S2A, B, C). The estimates of SAC coverage turned out virtually unchanged (Fig. S2D, E); SAC coverage by BC5o was still much lower than by BC5t and BC5i.

4.6 BC-SAC co-stratification analysis

Fig. 2D already showed that proximal SAC dendrites span a wide range of IPL depths, which are different from the depths of the intermediate and distal dendrites. Because of this depth difference, the proximal zone co-stratifies with BC7 but only weakly with BC5, which is consistent with our observed preference of BC7 for contact with the proximal zone. Such reasoning was already used by [Famiglietti(1991)] to infer that proximal dendrites should receive inputs from different BC types compared to distal dendrites.

This suggests that co-stratification could be used to quantitatively predict On BC-SAC contact using the integral over depth of the product of BC and SAC stratification profiles. Figure 5D shows that this prediction works well in some respects, but not in others. On the one hand, predicted contact (Fig. 5D) nicely matches actual contact (Fig. 5C) for BC5t, BC5i, and BC7, failing only to match the observed decrease in the distal zone. On the other hand, actual contact of BC6 is much lower than expected from predicted contact.

It may seem surprising that BC6 makes little contact with On SACs, given that it stratifies over a broad range of IPL depths that includes all zones of On SAC dendrites (Fig. 3A). One reason may be that the BC6 stratification profile dips down exactly at the depth of intermediate and distal dendrites (Fig. 3C), as if BC6 were trying to avoid contacting the On SAC.

4.7 Discussion

Our reconstruction of the On BC-SAC circuit suggests that its wiring diagram parallels that of the Off BC-SAC circuit (Fig. 1C). We find that sustained BC types prefer to contact SAC dendrites near the SAC soma, and transient BC types prefer an intermediate distance from the SAC soma. We interpret these contact preferences as reflecting synaptic connectivity preferences.

The spatial organization of the IPL has previously been interpreted as supporting rules of wiring specificity. For example, the division of the IPL into On and Off sublayers (Fig. 1A) supports On to On and Off to Off rules for wiring of BCs to ganglion cells (GCs) [Famiglietti and Kolb(1976a), Pang et al.(2003)Pang, Gao, and Wu]. Similarly, the division of the IPL into sustained and transient sublayers (Fig. 1B) could support sustained to sustained and transient to transient rules of BC-GC wiring [Awatramani and Slaughter(2000)]. Here the BC-SAC wiring diagram provides an explanation of why On and Off SACs are located at the boundaries between sustained and transient IPL sublayers (Fig. 1B). Namely, this positioning is appropriate for receiving convergent input from both sustained and transient BC types (Fig. 1C).

We also find three differences between the On and Off circuits. First, BC7 and BC5i/t prefer to contact closer to the On SAC soma than their analogs BC2 and BC3a contact to the Off SAC soma (compare Fig. 5C with Fig. 4d of [Kim et al.(2014)Kim, Greene, Zlateski, Lee, Richardson Second, the On SAC is contacted strongly by two transient BC types, while the Off SAC receives strong contact from a single transient BC type. Third, BC contact on distal

SAC dendrites is relatively scarcer for the On than the Off circuit (Fig. 2E).

The current study comes with several caveats. First, while most of the available evidence supports the sustained-transient classification of On BC types adopted in this paper [Baden et al.(2013)Baden, Berens, Bethge, and Euler, Borghuis et al.(2013)Borghuis, Marvin, Looger, and the literature contains at least one divergent report about this classification [Ichinose et al.(2014)Ichinose, Fyk Second, synaptic connectivity cannot be identified with certainty in e2198, because of an unconventional staining technique that left intracellular organelles invisible. Therefore we rely on contact between cells as an indirect indicator of connectivity. Third, motion computation by SAC dendrites might involve biophysics of SAC dendrites [Gavrikov et al.(2003)Gavrikov, Dmitr Tukker et al.(2004)Tukker, Taylor, and Smith, Hausselt et al.(2007)Hausselt, Euler, Detwiler, and Denk], which is not incompatible with our hypothetical mechanism involving space-time wiring specificity.

We were able to divide BC5 into three types (BC5t, BC5o, and BC5i), based on differences in stratification. Using patterns of contact with two ganglion cell types, we also replicated the prior two-way division by [Helmstaedter et al.(2013)Helmstaedter, Briggman, Turaga, Jain, S of BC5 into BC5A and BC5R, and found that BC5A corresponds almost perfectly with BC5i. We were able to assign all BC5 cells to either BC5A and BC5R, because our reconstructions of the ganglion cell types are more complete than those of [Helmstaedter et al.(2013)Helmstaedter, Briggman, Turaga, Jain, Seung, and Denk]. In the future, we expect contact or connectivity to replace stratification as the main property used to classify cells into types [Seung(2009), Seung(2012), Jonas and Kording(2015)].

[Wässle et al.(2009)Wässle, Puller, Müller, and Haverkamp] defined BC5 using a 5-HT3R-EGFP transgenic mouse line. They speculated that the line labeled two BC5 types, because of the high density of labeled cells, and because two BC5 types had been molecularly distinguished in rat [Fyk-Kolodziej and Pourcho(2007)]. However, they were unable to find molecular markers distinguishing BC5 types in mouse. [Duan et al.(2014)Duan, Krishnaswamy showed that Kcng4 and Cdh9 Cre lines label the same cells as 5-HT3R-EGFP. [Haverkamp et al.(2009)Haverk found that the BC5 cells in the 5-HT3R-EGFP line were all CaBP5-positive. BC5t may be CaBP5-negative (Haruhisa Okawa and Rachel Wong, private communication). If this is the case, it follows that BC5o and BC5i correspond to the two types in the 5-HT3R-EGFP transgenic line.

The catalog of mouse BC types is likely complete. Our claim is based on two assumptions: (1) every BC type tiles the retina with little overlap, and (2) there are no large BCs, which would be rare and therefore could have been missed by our reconstructions and those of [Helmstaedter et al.(2013)Helmstaedter, Briggman, Turaga, Jain, Seung, and Denk]. One anomaly is that BC1 and BC2 tilings exhibit more overlap than those of other types (Extended Data Figure 6 of [Kim et al.(2014)Kim, Greene, Zlateski, Lee, Richardson, Turaga, Purcaro, Bal The overlap is not enough to allow defining a third type that fully tiles the retina; a hypothetical third type would be sparse in its coverage. Another qualification is that our reconstructions come from a single location in a retina, so we cannot exclude the possibility that cell types vary across the retina.

4.8 Experimental Procedures

The methods of the present study are similar to those used previously [Kim et al.(2014)Kim, Greene, Zlateski
so the differences are the focus of the following text. As in the previous study, all dimen-
sions are uncorrected for shrinkage, which was previously estimated at 14% by comparison
of two-photon and serial electron microscopy images [Helmstaedter et al.(2013)Helmstaedter, Briggman, Tur

4.9 Alignment to a common coordinate system

In our previous study of the Off BC-SAC circuit [Kim et al.(2014)Kim, Greene, Zlateski, Lee, Richardson, Tu
we defined normalized coordinates that computationally flattened the Off SACs. In this
study we improved the coordinate system by additionally utilizing On SACs as land-
marks.

The volume was first rigidly transformed to minimize the averaged squared distance
of Off SACs to the xy plane. A rectangular 32×36 lattice was defined on the xy plane,
with nodes spaced at approximately 10 μm intervals. For each lattice node, we com-
puted the mean depth of all Off SAC surface voxels and the mean depth of all On SAC
surface voxels within a cylindrical neighborhood. Bilinear interpolation of these depths
yielded values $\mu_{x,y}^{OFF}$ and $\mu_{x,y}^{ON}$ for every point in the xy plane. Then the depth z of
every point (x, y, z) was transformed according to $z' = \left(z - \mu_{x,y}^{OFF}\right) / \left(\mu_{x,y}^{ON} - \mu_{x,y}^{OFF}\right)$,
yielding a coordinate system in which Off and On SACs are at depths 0 and 1, re-
spectively. Finally we linearly transformed to coordinates in which Off and On SACs
are at 0.28 and 0.62 IPL depth, respectively, for consistency with the definitions of
[Helmstaedter et al.(2013)Helmstaedter, Briggman, Turaga, Jain, Seung, and Denk].

4.10 SAC reconstruction

On SACs were reconstructed mostly during July 2013 to September 2014. EyeWirers
who helped reconstruct On SACs are listed in the Supplemental Information.

Off SACs were previously reconstructed both by forward tracing from the candidate
SAC soma to dendritic tips, and backward tracing from varicosities on candidate SAC
dendrites to the soma [Kim et al.(2014)Kim, Greene, Zlateski, Lee, Richardson, Turaga, Purcaro, Balkam, I
The forward method turned out to be less useful for On SACs because their dendrites
can take rather circuitous paths before reaching their final IPL depth and making the
distinctive starburst shape. Therefore it takes a great deal of reconstruction effort be-
fore a candidate cell can be accepted or rejected as a SAC. It saves human effort if this
decision can be made earlier in the reconstruction process. Two On SACs were recon-
structed by lab workers using the forward method. The remaining 75 were reconstructed
by EyeWirers using the backward method.

In a parallel study to be reported elsewhere, we exhaustively reconstructed all neurons
with somata in a $(200 \ \mu\text{m})^2$ GCL patch of e2198. This revealed 6 extra On SACs beyond
the 35 in the patch that had already been reconstructed for the present study. In other
words, the reconstructions of the present study had achieved 85% coverage of all On

SACs in this $(200\ \mu\mathrm{m})^2$ patch. Assuming that the density of On SACs is the same for all of e2198 as it is in the $(200\ \mu\mathrm{m})^2$ patch, the estimated number of On SACs in e2198 is roughly 110, and our overall coverage is roughly 70%. Our estimated coverage of Off SACs is slightly lower, as the Off SAC density is known to be slightly (less than 10%) larger than the On SAC density [Jeon et al.(1998)Jeon, Strettoi, and Masland].

4.11 SAC properties

Length of SAC dendrites (Fig. 2E inset) was calculated as the mean distance from the soma on the xy plane of the eight most distant points that are not within $30\,\mu$m of each other. These parameters were chosen because the points generated appeared to give an accurate representation of the dendritic length, while avoiding inaccuracy that arises from outliers and from dendrites that extend beyond the bounds of the volume.

4.12 BC reconstruction

On BCs were reconstructed mostly during February to December 2014. Because e2198 extends only partially into the INL, it was not possible to identify BCs based on the existence of a dendritic arbor in the OPL. Instead, we identified BC axonal arbors by comparison with [Helmstaedter et al.(2013)Helmstaedter, Briggman, Turaga, Jain, Seung, and Denk], who reconstructed all BCs in a patch of retina that included both IPL and OPL. BC axon candidates were neurites that pass through the interstices of the INL and emerge in the IPL. Many candidates could be immediately rejected as amacrine or ganglion cells because their arbors were too large, or rejected as glial cells based on surface concavity and roughness. Little human effort was necessary for these cases, because large parts of these cells were automatically reconstructed. The remaining candidates were put into the reconstruction pipeline, and were rejected as narrow field amacrine cells if their stratification profiles deviated markedly from those previously reported by [Helmstaedter et al.(2013)Helmstaedter, Briggman, Turaga, Jain, Seung, and Denk] for BCs. Eight were rejected in the middle of reconstruction, and three were rejected after full reconstruction.

4.13 BC classification

We define the stratification profile as the density of surface area versus depth in the IPL. For the purpose of BC classification, we restricted the domain of the stratification profile to the interval between IPL depth 0.4 and 1. The domain omitted depths between 0 and 0.4 to exclude the trunks of the axonal arbors, which increase variability of the stratification profiles. Each stratification profile is normalized like a probability density, so that profile area between IPL depths 0.4 and 1 integrates to unity. Since IPL depth is dimensionless, the stratification profile is also dimensionless. [Helmstaedter et al.(2013)Helmstaedter, Briggman, T defined stratification profile as the density of reconstructed skeleton. This definition is slightly different from ours, but yields similar results (data not shown). Percentiles are

defined for a stratification profile, in the same way as for a probability density. Namely, the interval from the nth percentile depth to 0th percentile depth contains n percent of the area of the stratification profile. As mentioned earlier, 0th percentile depth is defined as IPL depth 0.4. The thickness of the stratification profile is defined as the difference between 85th and 25th percentile depths. [Helmstaedter et al.(2013)Helmstaedter, Briggman, Turaga, Jain, Se defined thickness as the difference between 75th and 25th percentile depths, which yields similar classifications. In addition to stratification, we characterized single cell anatomy by a further property, the area of the cell's projection onto the tangential (xy) plane.

We hierarchically clustered our On BCs as follows. The axonal arbors of BC5 and XBC lie between the Off and On SACs. Accordingly, a BC5/XBC cluster separates from other types based on 85th percentile depth (Figure S1A). This cluster in turn subdivides by 25th percentile depth into outer (closer to the INL) and inner (closer to the GCL) clusters (Figure S1B). The outer cluster can be divided into BC5t and BC5o; the former is more thickly stratified than the latter (Figure S1D). The inner cluster divides into XBC and BC5i based on projection area (Figure S1E).

Types outside the BC5/XBC cluster lie between the On SACs and GCL. BC7 separates from the others by 85th percentile depth (Figure S1A). Then BC6, BC8/9, and RBC separate from each other based on projection area (Figure S1C). We chose not to separate BC8 and BC9, as the reconstructed cells were too few to yield two complete tilings.

BC8, BC9, and RBC all appear underrepresented relative to [Helmstaedter et al.(2013)Helmstaedter, Brigg This discrepancy could be artifactual, caused by failures to identify the relatively thin axons of these three types in the interstices of the INL. Alternatively, these cell types might be truly underrepresented in our volume.

Histograms showing the various splits in the hierarchical clustering are shown in Figure S1. The splits are highly convincing near the top of the hierarchy, but less convincing near the bottom. Therefore we sought further validation from the principle that the arbors of a bipolar cell type should "tile" the retina with little overlap. If the hierarchical clustering yields cell types that tile the retina, that would be independent validation of the clustering, which relied only on anatomical properties of single cells. For all types, few violations of the tiling principle were observed (Figure 3E, F, G). There are some holes in the tilings, but they are likely the result of omissions in cell reconstruction rather than classification errors. Violations of tiling can be rectified by swapping cells between types, to yield the improved classifications given in Fig. S3. The fraction of swapped cells is small (Table S1). Our final classification is exhibited in the "type gallery" of Fig. S3.

4.14 BC-SAC contact analysis

We only reconstructed BCs in the central area of e2198 (Fig. 1E), and even within this area some BCs may have been missed (Figs. 3E,F,G). In our previous paper, we described methods of analyzing BC-SAC contact that are robust to both kinds of incompleteness [Kim et al.(2014)Kim, Greene, Zlateski, Lee, Richardson, Turaga, Purcaro, Balkam, Robinson, Behabadi, (The same methods were applied here, with only minor changes.

We compute each SAC's total contact area with all BCs of a given type divided by the SAC's surface area contained in the convex hull of the same BCs. This yields an estimate of the fraction of the SAC's surface in contact with BCs of the given type. This fraction is averaged over SACs to yield the estimates shown in Fig. 5A, with standard error based on the number of SACs that intersect the convex hull of the given BC type.

For each BC type, a coverage factor is computed by dividing the sum of hull areas for cells of the given type by the area of the union of hulls of the cells. The coverage factor represents the extent to which neighboring BCs of the same type overlap one another.

For each BC-SAC pair, we compute the contact area divided by the surface area of the SAC within the convex hull of the BC. Multiplying by the coverage factor for the BC type yields an estimate of the fraction of the SAC's surface area contacting the BC type at that distance from that SAC's soma. This computation is done for all BC-SAC pairs, except that we discard pairs for which the BC hull contains fewer than 500 SAC surface voxels in order to dampen fluctuations. We bin the remaining BC-SAC pairs by distance and by BC type. For each bin and for each SAC that contributes pairs to that bin, we compute the mean over BC-SAC pairs. Each data point in Fig. 5C represents the mean of the SAC-specific means for that bin, and standard error is based on the number of SACs that contribute to that bin.

Figure S2 demonstrates the robustness of our analysis by showing that estimated SAC contact fractions change little even after randomly deleting many BCs.

The contact analysis was done with BC types given by hierarchical clustering after a small number of swaps to correct for tiling violations, as explained above and in Table S1. The results of the contact analysis look similar if the tiling swaps are not performed (data not shown).

5 DSGC Stuff?

asdasd

5.1 Identify synapses on SACs

adasd

5.2 BC-DSGC connections

adad

5.3 model

adasd

5.4 discussion

adas

Bibliography

[Adelson and Bergen(1985)] E H Adelson and J R Bergen. Spatiotemporal energy models for the perception of motion. *J Opt Soc Am A*, 2(2):284–99, Feb 1985.

[Amthor et al.(2002)Amthor, T, and Dmitrieva] Franklin R Amthor, Keyser Kent T, and Nina A Dmitrieva. Effects of the destruction of starburst-cholinergic amacrine cells by the toxin af64a on rabbit retinal directional selectivity. *Visual neuroscience*, 19(04):495–509, 2002.

[Awatramani and Slaughter(2000)] G B Awatramani and M M Slaughter. Origin of transient and sustained responses in ganglion cells of the retina. *J Neurosci*, 20(18): 7087–95, Sep 2000.

[Baccus and Meister(2002)] Stephen A Baccus and Markus Meister. Fast and slow contrast adaptation in retinal circuitry. *Neuron*, 36(5):909–19, Dec 2002.

[Baden et al.(2013)Baden, Berens, Bethge, and Euler] Tom Baden, Philipp Berens, Matthias Bethge, and Thomas Euler. Spikes in mammalian bipolar cells support temporal layering of the inner retina. *Curr Biol*, 23(1):48–52, 2013.

[Barlow and Levick(1965)] H B Barlow and W R Levick. The mechanism of directionally selective units in rabbit's retina. *J Physiol*, 178(3):477–504, Jun 1965.

[Barlow et al.(1964)Barlow, Hill, and Levick] H B Barlow, R M Hill, and W R Levick. Retinal ganglion cells responding selectively to direction and speed of image motion in the rabbit. *J Physiol*, 173:377–407, Oct 1964.

[Berry and Meister(1998)] M J Berry, II and M Meister. Refractoriness and neural precision. *J Neurosci*, 18(6):2200–11, Mar 1998.

[Binzegger et al.(2004)Binzegger, Douglas, and Martin] Tom Binzegger, Rodney J Douglas, and Kevan A C Martin. A quantitative map of the circuit of cat primary visual cortex. *J Neurosci*, 24(39):8441–53, Sep 2004. doi: 10.1523/JNEUROSCI.1400-04.2004.

[Borg-Graham and Grzywacz(1992)] Lyle J Borg-Graham and Norberto M Grzywacz. A model of the directional selectivity circuit in retina: transformations by neurons singly and in concert. In *Single neuron computation*, chapter 13, pages 347–76. Academic San Diego, 1992.

Bibliography

[Borghuis et al.(2013)Borghuis, Marvin, Looger, and Demb] Bart G Borghuis, Jonathan S Marvin, Loren L Looger, and Jonathan B Demb. Two-photon imaging of nonlinear glutamate release dynamics at bipolar cell synapses in the mouse retina. *J Neurosci*, 33(27):10972–85, 2013.

[Borst and Euler(2011)] Alexander Borst and Thomas Euler. Seeing things in motion: models, circuits, and mechanisms. *Neuron*, 71(6):974–94, Sep 2011. doi: 10.1016/j.neuron.2011.08.031.

[Borst et al.(2003)Borst, Reisenman, and Haag] Alexander Borst, Carolina Reisenman, and Juergen Haag. Adaptation of response transients in fly motion vision. II: Model studies. *Vision Res*, 43(11):1309–22, May 2003.

[Braitenberg and Schüz(1998)] Valentino Braitenberg and Almut Schüz. *Cortex: statistics and geometry of neuronal connectivity*. Springer Berlin, 2nd edition edition, 1998.

[Briggman et al.(2011)Briggman, Helmstaedter, and Denk] Kevin L Briggman, Moritz Helmstaedter, and Winfried Denk. Wiring specificity in the direction-selectivity circuit of the retina. *Nature*, 471(7337):183–8, Mar 2011. doi: 10.1038/nature09818.

[Chen et al.(2014)Chen, Lee, Park, Looger, and Zhou] Minggang Chen, Seunghoon Lee, Silvia J H Park, Loren L Looger, and Z Jimmy Zhou. Receptive field properties of bipolar cell axon terminals in direction-selective sublaminas of the mouse retina. *J Neurophysiol*, 112(8):1950–62, Oct 2014. doi: 10.1152/jn.00283.2014.

[Ciresan et al.(2012)Ciresan, Giusti, Schmidhuber, et al.] Dan Ciresan, Alessandro Giusti, Juergen Schmidhuber, et al. Deep neural networks segment neuronal membranes in electron microscopy images. In *Advances in Neural Information Processing Systems 25*, pages 2852–2860, 2012.

[Cooper et al.(2010)Cooper, Khatib, Treuille, Barbero, Lee, Beenen, Leaver-Fay, Baker, Popović, and Playe Seth Cooper, Firas Khatib, Adrien Treuille, Janos Barbero, Jeehyung Lee, Michael Beenen, Andrew Leaver-Fay, David Baker, Zoran Popović, and Foldit Players. Predicting protein structures with a multiplayer online game. *Nature*, 466(7307): 756–60, Aug 2010. doi: 10.1038/nature09304.

[Dowling and Boycott(1966)] JE Dowling and BB Boycott. Organization of the primate retina: electron microscopy. *Proceedings of the Royal Society of London B: Biological Sciences*, 166(1002):80–111, 1966.

[Duan et al.(2014)Duan, Krishnaswamy, De la Huerta, and Sanes] Xin Duan, Arjun Krishnaswamy, Irina De la Huerta, and Joshua R Sanes. Type ii cadherins guide assembly of a direction-selective retinal circuit. *Cell*, 158(4):793–807, Aug 2014. doi: 10.1016/j.cell.2014.06.047.

Bibliography

[Euler et al.(2002)Euler, Detwiler, and Denk] Thomas Euler, Peter B Detwiler, and Winfried Denk. Directionally selective calcium signals in dendrites of starburst amacrine cells. *Nature*, 418(6900):845–52, 2002.

[Famiglietti(1991)] E V Famiglietti. Synaptic organization of starburst amacrine cells in rabbit retina: analysis of serial thin sections by electron microscopy and graphic reconstruction. *J Comp Neurol*, 309(1):40–70, Jul 1991. doi: 10.1002/cne.903090105.

[Famiglietti(1983)] E V Famiglietti, Jr. On and off pathways through amacrine cells in mammalian retina: the synaptic connections of "starburst" amacrine cells. *Vision Res*, 23(11):1265–79, 1983.

[Famiglietti and Kolb(1976a)] E V Famiglietti, Jr and H Kolb. Structural basis for on- and off-center responses in retinal ganglion cells. *Science*, 194(4261):193–5, Oct 1976a.

[Famiglietti(1981)] Edward V Famiglietti. Functional architecture of cone bipolar cells in mammalian retina. *Vision research*, 21(11):1559–1563, 1981.

[Famiglietti and Kolb(1976b)] EV Famiglietti and Helga Kolb. Structural basis for on- and off-center responses in retinal ganglion cells. *Science*, 194(4261):193–195, 1976b.

[Famiglietti et al.(1977)Famiglietti, Kaneko, and Tachibana] EV Famiglietti, Akimichi Kaneko, and Masao Tachibana. Neuronal architecture of on and off pathways to ganglion cells in carp retina. *Science*, 198(4323):1267–1269, 1977.

[Fiala(2005)] J C Fiala. Reconstruct: a free editor for serial section microscopy. *J Microsc*, 218(Pt 1):52–61, Apr 2005. doi: 10.1111/j.1365-2818.2005.01466.x.

[Fried et al.(2002)Fried, Münch, and Werblin] Shelley I Fried, Thomas A Münch, and Frank S Werblin. Mechanisms and circuitry underlying directional selectivity in the retina. *Nature*, 420(6914):411–4, Nov 2002. doi: 10.1038/nature01179.

[Fyk-Kolodziej and Pourcho(2007)] Bozena Fyk-Kolodziej and Roberta G Pourcho. Differential distribution of hyperpolarization-activated and cyclic nucleotide-gated channels in cone bipolar cells of the rat retina. *Journal of Comparative Neurology*, 501(6):891–903, 2007.

[Gavrikov et al.(2003)Gavrikov, Dmitriev, Keyser, and Mangel] Konstantin E Gavrikov, Andrey V Dmitriev, Kent T Keyser, and Stuart C Mangel. Cation–chloride cotransporters mediate neural computation in the retina. *Proc Natl Acad Sci U S A*, 100 (26):16047–52, Dec 2003. doi: 10.1073/pnas.2637041100.

[Ghosh et al.(2004)Ghosh, Bujan, Haverkamp, Feigenspan, and Wässle] Krishna K Ghosh, Sascha Bujan, Silke Haverkamp, Andreas Feigenspan, and Heinz Wässle. Types of bipolar cells in the mouse retina. *J Comp Neurol*, 469(1):70–82, Jan 2004. doi: 10.1002/cne.10985.

[Hausselt et al.(2007)Hausselt, Euler, Detwiler, and Denk] Susanne E Hausselt, Thomas Euler, Peter B Detwiler, and Winfried Denk. A dendrite-autonomous mechanism for direction selectivity in retinal starburst amacrine cells. *PLoS Biol.*, 5(7):e185, 2007.

[Haverkamp et al.(2009)Haverkamp, Inta, Monyer, and Wässle] S Haverkamp, D Inta, H Monyer, and H Wässle. Expression analysis of green fluorescent protein in retinal neurons of four transgenic mouse lines. *Neuroscience*, 160(1):126–139, 2009.

[Helmstaedter et al.(2013)Helmstaedter, Briggman, Turaga, Jain, Seung, and Denk] Moritz Helmstaedter, Kevin L Briggman, Srinivas C Turaga, Viren Jain, H Sebastian Seung, and Winfried Denk. Connectomic reconstruction of the inner plexiform layer in the mouse retina. *Nature*, 500(7461):168–74, Aug 2013. doi: 10.1038/nature12346.

[Ichinose et al.(2014)Ichinose, Fyk-Kolodziej, and Cohn] Tomomi Ichinose, Bozena Fyk-Kolodziej, and Jesse Cohn. Roles of on cone bipolar cell subtypes in temporal coding in the mouse retina. *J Neurosci*, 34(26):8761–71, Jun 2014. doi: 10.1523/JNEUROSCI.3965-13.2014.

[Jeon et al.(1998)Jeon, Strettoi, and Masland] Chang-Jin Jeon, Enrica Strettoi, and Richard H. Masland. The major cell populations of the mouse retina. *J Neurosci*, 18(21):8936–8946, Aug 1998.

[Jonas and Kording(2015)] Eric Jonas and Konrad Kording. Automatic discovery of cell types and microcircuitry from neural connectomics. *eLife*, 4:e04250, 2015.

[Kalisman et al.(2003)Kalisman, Silberberg, and Markram] Nir Kalisman, Gilad Silberberg, and Henry Markram. Deriving physical connectivity from neuronal morphology. *Biol Cybern*, 88(3):210–8, Mar 2003. doi: 10.1007/s00422-002-0377-3.

[Kaneko(1970)] Akimichi Kaneko. Physiological and morphological identification of horizontal, bipolar and amacrine cells in goldfish retina. *The Journal of physiology*, 207 (3):623–633, 1970.

[Kim et al.(2008)Kim, Zhang, Yamagata, Meister, and Sanes] In-Jung Kim, Yifeng Zhang, Masahito Yamagata, Markus Meister, and Joshua R Sanes. Molecular identification of a retinal cell type that responds to upward motion. *Nature*, 452 (7186):478–82, Mar 2008. doi: 10.1038/nature06739.

[Kim et al.(2014)Kim, Greene, Zlateski, Lee, Richardson, Turaga, Purcaro, Balkam, Robinson, Behabadi, C Jinseop S Kim, Matthew J Greene, Aleksandar Zlateski, Kisuk Lee, Mark Richardson, Srinivas C Turaga, Michael Purcaro, Matthew Balkam, Amy Robinson, Bardia F Behabadi, Michael Campos, Winfried Denk, H Sebastian Seung, and the EyeWirers. Space-time wiring specificity supports direction selectivity in the retina. *Nature*, 509(7500):331–6, May 2014. doi: 10.1038/nature13240.

[Lagnado et al.(1996)Lagnado, Gomis, and Job] L Lagnado, A Gomis, and C Job. Continuous vesicle cycling in the synaptic terminal of retinal bipolar cells. *Neuron*, 17 (5):957–67, Nov 1996.

[Lee and Zhou(2006)] Seunghoon Lee and Z Jimmy Zhou. The synaptic mechanism of direction selectivity in distal processes of starburst amacrine cells. *Neuron*, 51(6): 787–99, Sep 2006. doi: 10.1016/j.neuron.2006.08.007.

[Lettvin et al.(1959)Lettvin, Maturana, McCulloch, and Pitts] Jerome Y Lettvin, Humberto R Maturana, Warren S McCulloch, and Walter H Pitts. What the frog's eye tells the frog's brain. *Proceedings of the IRE*, 47(11):1940–1951, 1959.

[Lintott et al.(2008)Lintott, Schawinski, Slosar, Land, Bamford, Thomas, Raddick, Nichol, Szalay, Andreescu] C.J. Lintott, K. Schawinski, A. Slosar, K. Land, S. Bamford, D. Thomas, M.J. Raddick, R.C. Nichol, A. Szalay, D. Andreescu, et al. Galaxy Zoo: morphologies derived from visual inspection of galaxies from the Sloan Digital Sky Survey. *Monthly Notices of the Royal Astronomical Society*, 389(3):1179–1189, 2008.

[Maisak et al.(2013)Maisak, Haag, Ammer, Serbe, Meier, Leonhardt, Schilling, Bahl, Rubin, Nern, Dickson] Matthew S Maisak, Juergen Haag, Georg Ammer, Etienne Serbe, Matthias Meier, Aljoscha Leonhardt, Tabea Schilling, Armin Bahl, Gerald M Rubin, Aljoscha Nern, Barry J Dickson, Dierk F Reiff, Elisabeth Hopp, and Alexander Borst. A directional tuning map of drosophila elementary motion detectors. *Nature*, 500(7461):212–6, Aug 2013. doi: 10.1038/nature12320.

[Manookin et al.(2008)Manookin, Beaudoin, Ernst, Flagel, and Demb] Michael B Manookin, Deborah Langrill Beaudoin, Zachary Raymond Ernst, Leigh J Flagel, and Jonathan B Demb. Disinhibition combines with excitation to extend the operating range of the off visual pathway in daylight. *J Neurosci*, 28(16):4136–50, Apr 2008. doi: 10.1523/JNEUROSCI.4274-07.2008.

[Masland(2004)] Richard H Masland. Neuronal cell types. *Current Biology*, 14(13): R497–R500, 2004.

[Mills and Massey(1992)] Stephen L Mills and Stephen C Massey. Morphology of bipolar cells labeled by dapi in the rabbit retina. *Journal of Comparative Neurology*, 321 (1):133–149, 1992.

[Missotten(1965)] L Missotten. The synapses in the human retina. In *The structure of the eye*, volume 2, pages 17–28. Schattauer-Verlag Stuttgart, 1965.

[Münch and Werblin(2006)] Thomas A Münch and Frank S Werblin. Symmetric interactions within a homogeneous starburst cell network can lead to robust asymmetries in dendrites of starburst amacrine cells. *J Neurophysiol*, 96(1):471–7, Jul 2006. doi: 10.1152/jn.00628.2005.

Bibliography

[Mutch et al.(2010)Mutch, Knoblich, and Poggio] Jim Mutch, Ulf Knoblich, and Tomaso Poggio. CNS: a GPU-based framework for simulating cortically-organized networks. Technical Report MIT-CSAIL-TR-2010-013 / CBCL-286, Massachusetts Institute of Technology, Cambridge, MA, February 2010.

[Nelson et al.(1978)Nelson, Famiglietti, and Kolb] R Nelson, EV Famiglietti, and H Kolb. Intracellular staining reveals different levels of stratification for on-and off-center ganglion cells in cat retina. *Journal of Neurophysiology*, 41(2):472–483, 1978.

[Oesch and Taylor(2010)] Nicholas W Oesch and W Rowland Taylor. Tetrodotoxin-resistant sodium channels contribute to directional responses in starburst amacrine cells. *PLoS One*, 5(8):e12447, 2010. doi: 10.1371/journal.pone.0012447.

[Pang et al.(2003)Pang, Gao, and Wu] Ji-Jie Pang, Fan Gao, and Samuel M Wu. Light-evoked excitatory and inhibitory synaptic inputs to on and off α ganglion cells in the mouse retina. *The Journal of neuroscience*, 23(14):6063–6073, 2003.

[Rall(1964)] Wilfrid Rall. Theoretical significance of dendritic trees for neuronal input-output relations. In R. F. Reis, editor, *Neural theory and modeling*, pages 73–97. Stanford Univ. Press, 1964.

[Reichardt(1961)] Werner Reichardt. Autocorrelation, a principle for the evaluation of sensory information by the central nervous system. In *Sensory communication*, pages 303–317. 1961.

[Seung(2009)] H Sebastian Seung. Reading the book of memory: sparse sampling versus dense mapping of connectomes. *Neuron*, 62(1):17–29, 2009.

[Seung and Sümbül(2014)] H Sebastian Seung and Uygar Sümbül. Neuronal cell types and connectivity: lessons from the retina. *Neuron*, 83(6):1262–72, Sep 2014. doi: 10.1016/j.neuron.2014.08.054.

[Seung(2012)] Sebastian Seung. *Connectome: How the brain's wiring makes us who we are*. Houghton Mifflin Harcourt, 2012.

[Siegert et al.(2009)Siegert, Scherf, Del Punta, Didkovsky, Heintz, and Roska] Sandra Siegert, Brigitte Gross Scherf, Karina Del Punta, Nick Didkovsky, Nathaniel Heintz, and Botond Roska. Genetic address book for retinal cell types. *Nat Neurosci*, 12 (9):1197–204, Sep 2009. doi: 10.1038/nn.2370.

[Stepanyants and Chklovskii(2005)] Armen Stepanyants and Dmitri B Chklovskii. Neurogeometry and potential synaptic connectivity. *Trends Neurosci*, 28(7):387–94, Jul 2005. doi: 10.1016/j.tins.2005.05.006.

[Sümbül et al.(2014)Sümbül, Song, McCulloch, Becker, Lin, Sanes, Masland, and Seung] Uygar Sümbül, Sen Song, Kyle McCulloch, Michael Becker, Bin Lin, Joshua R Sanes, Richard H Masland, and H Sebastian Seung. A genetic and computational

approach to structurally classify neuronal types. *Nat Commun*, 5:3512, 2014. doi: 10.1038/ncomms4512.

[Surowiecki(2005)] James Surowiecki. *The Wisdom of Crowds*. Anchor, 2005.

[Takemura et al.(2013)Takemura, Bharioke, Lu, Nern, Vitaladevuni, Rivlin, Katz, Olbris, Plaza, Winston, Shin-ya Takemura, Arjun Bharioke, Zhiyuan Lu, Aljoscha Nern, Shiv Vitaladevuni, Patricia K Rivlin, William T Katz, Donald J Olbris, Stephen M Plaza, Philip Winston, Ting Zhao, Jane Anne Horne, Richard D Fetter, Satoko Takemura, Katerina Blazek, Lei-Ann Chang, Omotara Ogundeyi, Mathew A Saunders, Victor Shapiro, Christopher Sigmund, Gerald M Rubin, Louis K Scheffer, Ian A Meinertzhagen, and Dmitri B Chklovskii. A visual motion detection circuit suggested by Drosophila connectomics. *Nature*, 500(7461):175–81, Aug 2013. doi: 10.1038/nature12450.

[Tukker et al.(2004)Tukker, Taylor, and Smith] John J Tukker, W Rowland Taylor, and Robert G Smith. Direction selectivity in a model of the starburst amacrine cell. *Visual neuroscience*, 21(4):611–625, 2004.

[Turaga et al.(2009)Turaga, Briggman, Helmstaedter, Denk, and Seung] Srinivas Turaga, Kevin Briggman, Moritz Helmstaedter, Winfried Denk, and Sebastian Seung. Maximin affinity learning of image segmentation. In Y. Bengio, D. Schuurmans, J. Lafferty, C. K. I. Williams, and A. Culotta, editors, *Advances in Neural Information Processing Systems 22*, pages 1865–1873. 2009.

[Turaga et al.(2010)Turaga, Murray, Jain, Roth, Helmstaedter, Briggman, Denk, and Seung] Srinivas C Turaga, Joseph F Murray, Viren Jain, Fabian Roth, Moritz Helmstaedter, Kevin Briggman, Winfried Denk, and H Sebastian Seung. Convolutional networks can learn to generate affinity graphs for image segmentation. *Neural Comput*, 22 (2):511–38, Feb 2010. doi: 10.1162/neco.2009.10-08-881.

[Vaney et al.(2012)Vaney, Sivyer, and Taylor] David I Vaney, Benjamin Sivyer, and W Rowland Taylor. Direction selectivity in the retina: symmetry and asymmetry in structure and function. *Nat. Rev. Neurosci*, 13(3):194–208, Mar 2012. doi: 10.1038/nrn3165.

[Vlasits et al.(2014)Vlasits, Bos, Morrie, Fortuny, Flannery, Feller, and Rivlin-Etzion] Anna L Vlasits, Rémi Bos, Ryan D Morrie, Cécile Fortuny, John G Flannery, Marla B Feller, and Michal Rivlin-Etzion. Visual stimulation switches the polarity of excitatory input to starburst amacrine cells. *Neuron*, 83(5):1172–84, Sep 2014. doi: 10.1016/j.neuron.2014.07.037.

[Von Ahn and Dabbish(2004)] Luis Von Ahn and Laura Dabbish. Labeling images with a computer game. In *Proceedings of the SIGCHI conference on human factors in computing systems*, pages 319–326. ACM, 2004.

[Wässle et al.(2009)Wässle, Puller, Müller, and Haverkamp] H. Wässle, C. Puller, F. Müller, and S. Haverkamp. Cone contacts, mosaics, and territories of bipolar cells in the mouse retina. *The Journal of Neuroscience*, 29(1):106–117, 2009.

[Watson and Ahumada(1985)] A B Watson and A J Ahumada, Jr. Model of human visual-motion sensing. *J Opt Soc Am A*, 2(2):322–41, Feb 1985.

[Wei et al.(2010)Wei, Hamby, Zhou, and Feller] Wei Wei, Aaron M Hamby, Kaili Zhou, and Marla B Feller. Development of asymmetric inhibition underlying direction selectivity in the retina. *Nature*, 469(7330):402–406, 2010.

[Werblin and Dowling(1969)] FRANK S Werblin and JOHN E Dowling. Organization of the retina of the mudpuppy, necturus maculosus. ii. intracellular recording. *Journal of neurophysiology*, 32(3):339–355, 1969.

[West(1978)] Roger W West. Bipolar and horizontal cells of the gray squirrel retina: Golgi morphology and receptor connections. *Vision Research*, 18(2):129–136, 1978.

[White et al.(1986)White, Southgate, Thomson, and Brenner] J G White, E Southgate, J N Thomson, and S Brenner. The structure of the nervous system of the nematode caenorhabditis elegans. *Philos Trans R Soc Lond B Biol Sci*, 314(1165):1–340, Nov 1986.

[Wiesel(1960)] TN Wiesel. Receptive fields of ganglion cells in the cat's retina. *The Journal of physiology*, 153(3):583–594, 1960.

[Wolbarsht et al.(1961)Wolbarsht, Wagner, and MacNichol Jr] ML Wolbarsht, HG Wagner, and EF MacNichol Jr. Receptive fields of retinal ganglion cells: extent and spectral sensitivity. In *Neurophysiologie und Psychophysik des Visuellen Systems/The Visual System: Neurophysiology and Psychophysics*, pages 170–177. Springer, 1961.

[Wyatt and Daw(1975)] Harry J Wyatt and Nigel W Daw. Directionally sensitive ganglion cells in the rabbit retina: specificity for stimulus direction, size, and speed. *Journal of Neurophysiology*, 38(3):613–626, 1975.

[Yonehara et al.(2010)Yonehara, Balint, Noda, Nagel, Bamberg, and Roska] Keisuke Yonehara, Kamill Balint, Masaharu Noda, Georg Nagel, Ernst Bamberg, and Botond Roska. Spatially asymmetric reorganization of inhibition establishes a motion-sensitive circuit. *Nature*, 469(7330):407–410, 2010.

[Yonehara et al.(2013)Yonehara, Farrow, Ghanem, Hillier, Balint, Teixeira, Jüttner, Noda, Neve, Conzelma Keisuke Yonehara, Karl Farrow, Alexander Ghanem, Daniel Hillier, Kamill Balint, Miguel Teixeira, Josephine Jüttner, Masaharu Noda, Rachael L Neve, Karl-Klaus Conzelmann, and Botond Roska. The first stage of cardinal direction selectivity is localized to the dendrites of retinal ganglion cells. *Neuron*, 79(6):1078–85, Sep 2013. doi: 10.1016/j.neuron.2013.08.005.

[Yoshida et al.(2001)Yoshida, Watanabe, Ishikane, Tachibana, Pastan, and Nakanishi] K Yoshida, D Watanabe, H Ishikane, M Tachibana, I Pastan, and S Nakanishi. A key role of starburst amacrine cells in originating retinal directional selectivity and optokinetic eye movement. *Neuron*, 30(3):771–80, Jun 2001.

Bibliography

[Zhou and Lee(2008)] Z Jimmy Zhou and Seunghoon Lee. Synaptic physiology of direction selectivity in the retina. *J Physiol*, 586(Pt 18):4371–6, Sep 2008. doi: 10.1113/jphysiol.2008.159020.